

INTERIM REPORT

AQUEOUS MINERAL CARBONATION

Mineral Availability, Pretreatment, Reaction
Parametrics, And Process Studies

September 30, 2004

By

W.K. O'Connor, D.C. Dahlin, G.E. Rush, S.J. Gerdemann,
L.R. Penner, and D.N. Nilsen

Office of Process Development
Albany Research Center
Office of Fossil Energy, US DOE



Office of Fossil Energy, U.S. Dept. of Energy

TABLE OF CONTENTS

| | <i>Page</i> |
|---|-------------|
| Abstract..... | 1 |
| Introduction..... | 1 |
| Mineral Chemistry..... | 1 |
| Carbonation Reactions..... | 1 |
| Carbonation Potential..... | 1 |
| Carbonation Reactivity..... | 1 |
| Mineral Availability..... | 2 |
| Ultramafic Mineral Carbonation Regions..... | 2 |
| Coal Consumption and Ore Tonnage..... | 3 |
| Ultramafic Mineral Resources..... | 3 |
| Mafic Mineral Carbonation Regions..... | 3 |
| Mineral Pretreatment..... | 4 |
| Mechanical Activation..... | 5 |
| Thermal Activation..... | 5 |
| Energy Consumption..... | 7 |
| Physical Properties..... | 8 |
| Reaction Parametrics..... | 8 |
| Experimental Procedure and Apparatus..... | 8 |
| Carbonation Carrier Solution..... | 10 |
| Carbonic Acid System..... | 10 |
| Bicarbonate System..... | 10 |
| Carrier Solution pH..... | 11 |
| Thermodynamics..... | 11 |
| Ca-Silicate Carrier Solution..... | 12 |
| Carbonation Temperature and Pressure..... | 12 |
| Optimized Carbonation Conditions..... | 13 |
| Process Development..... | 13 |
| Mineral Carbonation History..... | 13 |
| Reactor Design..... | 13 |
| Process Feasibility Study..... | 14 |
| Carbonation Costs..... | 15 |
| Discussion..... | 16 |
| Carbonation Costs..... | 16 |
| CO ₂ Balance..... | 16 |
| Recoverable Values..... | 17 |
| Conclusion..... | 18 |
| References..... | 19 |

TABLE OF CONTENTS

| | <i>Page</i> |
|---|-------------|
| Appendix A: Sample ID and Grinding History..... | A1 |
| Appendix B: Pretreatment History..... | B1 |
| Appendix C: Carbonation Parametric Space Conditions..... | C1 |
| Appendix D: Carbonation Results..... | D1 |
| Appendix E: Comments and Observations..... | E1 |
| Appendix F: Feed and Product Chemistry, Solids and Solutions..... | F1 |
| Appendix G: Mass and elemental balances for a selection of carbonation tests..... | G1 |

LIST OF TABLES

| | <i>Page</i> |
|--|-------------|
| Table I. Mineral chemistry, carbonation potential, and reactivity..... | 2 |
| Table II. Annual coal consumption, CO ₂ emissions, and ore demand by mineral carbonation region..... | 4 |
| Table III. Annual coal consumption, CO ₂ emissions, and ore demand by mafic mineral carbonation region..... | 4 |
| Table IV. Energy consumption by feed material and specific pretreatment methodology..... | 7 |
| Table V. Parasitic energy loss by pretreatment..... | 7 |
| Table VI. Physical properties of the pretreatment products..... | 8 |
| Table VII. Carrier solution, pH and R _x ¹ | 11 |
| Table VIII. Optimum carbonation conditions, by mineral..... | 13 |
| Table IX. Annual coal consumption, energy generation, CO ₂ emissions, ore requirements, and carbonation costs by ultramafic mineral carbonation region..... | 16 |
| Table X. Energy consumption for the mineral carbonation process, with derived CO ₂ avoided..... | 17 |
| Table XI. By-product iron ore value..... | 17 |

LIST OF FIGURES

| | <i>Page</i> |
|---|-------------|
| Figure 1. Ultramafic mineral carbonation regions..... | 3 |
| Figure 2. Mafic mineral carbonation regions..... | 3 |
| Figure 3. Grinding energy versus R_x | 5 |
| Figure 4. Olivine grinding energy versus particle size and surface area..... | 5 |
| Figure 5. DTA (red) & TGA (black) for antigorite..... | 5 |
| Figure 6. Antigorite heat treatment energy versus R_x | 6 |
| Figure 7. Schematic of laboratory apparatus..... | 9 |
| Figure 8. Carbon dioxide species distribution diagram..... | 11 |
| Figure 9. Gibbs free energy of formation for a selection of carbonation reactions, @ 1 atm CO_2 | 11 |
| Figure 10A. Carbonation temperature sensitivity diagram..... | 12 |
| Figure 10B. Carbonation P_{CO_2} sensitivity diagram..... | 12 |
| Figure 11. Conceptual pipeline reactor..... | 13 |
| Figure 12. Laboratory-scale flow loop reactor..... | 13 |
| Figure 13. Aqueous mineral carbonation process..... | 14 |
| Figure 14. Conventional reactor design used in feasibility study..... | 14 |

ABSTRACT

Aqueous mineral carbonation has been studied at the Albany Research Center as a potential option for CO₂ sequestration. The research has included fundamental studies, resource evaluation, and process development. Studies have focused on the reaction of Ca-, Fe-, and Mg-silicate minerals with gaseous CO₂ to form geologically stable, naturally occurring solid carbonate minerals. Process development has progressed in parallel with an economic evaluation, with an initial overall cost estimate of ~\$69/ton CO₂. Improved mineral pretreatment and reactor design indicate that costs could be reduced. However, the scale of ex-situ operations, requiring ~55 kt mineral/day to carbonate 100% of the CO₂ emissions from a 1 GW coal-fired power plant, may favor an in-situ methodology. Laboratory studies of in-situ mineral carbonation show promise.

INTRODUCTION

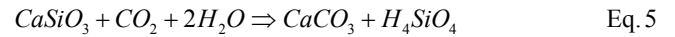
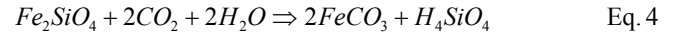
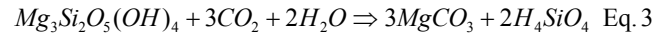
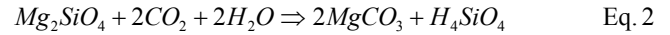
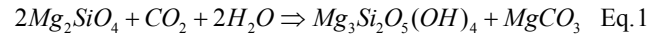
Carbon dioxide sequestration by mineral carbonation has been investigated for the past five years at the Albany Research Center (ARC), in collaboration with the Office of Fossil Energy - Mineral Carbonation Study Group. This work has focused on the development of an *ex situ* aqueous process to convert magnesium silicate-rich ultramafic rocks and minerals, such as olivine and serpentine, to magnesium carbonates by contact with gaseous CO₂ in an aqueous solution. Studies within the last year have been expanded to include alternative mineral feed stocks, including calcium- and ferrous iron-rich rocks and minerals, including wollastonite and basalt. Initial studies using ultramafic rocks simplified the reaction sequence by providing high-purity mineral reactants with high concentrations of the primary cations (Ca, Fe²⁺, Mg) necessary for precipitation of stable carbonate compounds, such as calcite (CaCO₃), siderite (FeCO₃), and magnesite (MgCO₃). Emphasis has been placed on the energy consumption for the overall process, which is impacted most significantly by reaction kinetics, parameters, and efficiency. Because all three are dependent upon the mineral reactants used, some discussion of these reactants is warranted.

MINERAL CHEMISTRY

Carbonation Reactions

The alteration of Mg-bearing ultramafic rocks by natural hydrothermal fluids is known as serpentinization, and produces hydrated Mg-silicate minerals (serpentine) and, when CO₂ is available, magnesite (eq. 1). Increasing the activity of CO₂ can by-pass the formation of the hydrated species to form the carbonates and silicic acid and/or free silica (eq. 2). Because this reaction occurs in nature and is thermodynamically favored, it became the basis for the aqueous mineral carbonation process. Studies demonstrated that the list of primary mineral

reactants could be expanded beyond the Mg-rich silicates to include the Ca- and Fe²⁺-rich silicates as well. The theoretical carbonation reactions for the Ca-, Fe²⁺-, and Mg-silicates are included below for reference (eq. 1-5).



Carbonation Potential

A key theoretical yardstick for the value of a particular mineral reactant for mineral carbonation is its carbonation potential. The carbonation potential for a rock or mineral was described by Goff et al. (2000) regarding the hydrated magnesium silicate serpentine [Mg₃Si₂O₅(OH)₄]. Goff used the molar concentration of Mg in a serpentine sample to calculate the theoretical number of moles of CO₂ that could be converted to magnesite (MgCO₃) by reaction with the serpentine. This method was modified for the current study to include the cations Ca and Fe²⁺ in the calculation, because all three cations can potentially form stable carbonate compounds. The modified method thus permits the calculation of the carbonation potential for the alternative mineral feed stocks studied (Table I). The carbonation potential, R_{CO₂}, was calculated from the total molar concentration of Ca, Fe²⁺, and Mg in the feed, and is defined here as the mass ratio of rock or mineral necessary to convert a unit mass of CO₂ to the solid carbonate (eq. 6). By this definition, a low R_{CO₂} is preferable to a high R_{CO₂}.

$$R_{CO_2} = \frac{100}{\left(\sum Ca^{2+} + Fe^{2+} + Mg^{2+}\right) MW_{CO_2}} \quad \text{Eq. 6}$$

Where:

$\sum Ca^{2+} + Fe^{2+} + Mg^{2+}$ = The sum of the molar concentrations for the specified cations.

MW_{CO_2} = Molecular weight of CO₂.

Carbonation Reactivity

While the R_{CO₂} is an inherent property of a rock or mineral, based strictly on its chemical composition, the carbonation reactivity of that rock or mineral is dependent on numerous factors, including the mineral composition, pretreatment, and solubility at the specific carbonation conditions of time, temperature, and pressure.

An evaluation of the relative sequestration reactivity for the specific mineral feed stocks studied is also included in Table I. The reactivity of the various feed materials was measured as the extent of reaction, R_x, or the percent stoichiometric conversion of the Ca-, Fe²⁺-, and Mg-silicates to their carbonate counterparts (eq. 7).

Table I. Mineral chemistry, carbonation potential, and reactivity.¹

| Rock/mineral group | Mineral | Formula | Concentration, wt pct | | | | R _{CO₂} ² | ε _A , % | R _X ³ , % |
|--------------------|-------------------|---|-----------------------|------------------|------|-----------------|--|--------------------|---------------------------------|
| | | | Feed | | | Prod. | | | |
| | | | Ca | Fe ²⁺ | Mg | CO ₂ | | | |
| Feldspar | Anorthite (An) | CaAl ₂ Si ₂ O ₈ | 10.3 | 3.1 | 4.8 | 1.9 | 4.4 | 23 | 9 |
| Serpentine | Antigorite (Ant) | Mg ₃ Si ₂ O ₅ (OH) ₄ | <0.1 | 2.4 | 24.6 | 24.2 | 2.1 | 47 | 92 |
| Pyroxene | Augite (Aug) | CaMgSi ₂ O ₆ + (Fe,Al) | 15.6 | 9.6 | 6.9 | 11.1 | 2.7 | 37 | 33 |
| Basalt | An, Aug, Mt, Ol | | 6.7 | 6.7 | 4.3 | 2.9 | 4.9 | 37 | 15 |
| Olivine (Ol) | Fayalite (Fa) | Fe ₂ SiO ₄ | 0.6 | 44.3 | 0.3 | 19.2 | 2.8 | 36 | 66 |
| Olivine (Ol) | Forsterite (Fo) | Mg ₂ SiO ₄ | 0.1 | 6.1 | 27.9 | 29.7 | 1.8 | 56 | 81 |
| Serpentine | Lizardite (Liz) | Mg ₃ Si ₂ O ₅ (OH) ₄ | 0.3 | 1.5 | 20.7 | 16.0 | 2.5 | 39 | 40 |
| Oxide | Magnetite (Mt) | Fe ₃ O ₄ | 0.6 | 21.9 | 0.3 | 1.5 | 5.5 | 18 | 08 |
| Ultramafic | Talc | Mg ₃ Si ₄ O ₁₀ (OH) ₂ | 2.2 | 9.2 | 15.7 | 5.2 | 2.8 | 36 | 15 |
| Ultramafic | Wollastonite (Wo) | CaSiO ₃ | 31.6 | 0.5 | 0.3 | 22.9 | 2.8 | 36 | 82 |

¹ Carbonation test conditions: 80% -37 μm feed; 1 hour; 185°C; P_{CO₂}=150 atm; 15% solids; 0.64 M NaHCO₃, 1 M NaCl.

² Mass ratio of ore necessary to carbonate unit mass of CO₂.

³ Reaction efficiency, percent stoichiometric conversion of Ca, Fe²⁺, and Mg cations in silicate feed to carbonate.

$$R_X = \frac{X_{CO_2}}{\epsilon_A(1 - X_{CO_2})} \quad \text{Eq. 7}$$

Where:

X_{CO_2} = CO₂ concentration in the solid products in weight percent.

ε_A = Percent weight gain assuming 100% stoichiometric conversion of the available cations to the carbonates.

Due to the variability in mineral solubility, partial pressure of CO₂ (P_{CO₂}) sensitivity, and precipitation kinetics, it was not practical to conduct all tests at a standardized set of pretreatment and carbonation conditions. Thus, the R_X values reported in Table I generally represent the best results achieved for each mineral reactant to date. The standardized test conditions are included as a footnote to the table. Variations from the standard conditions are noted below. For example, the wollastonite and forsterite exhibit comparable R_X, but both required an ultra-fine grinding pretreatment stage to achieve those reaction efficiencies. In addition, the P_{CO₂} for the wollastonite carbonation is much lower than that for the forsterite, at 40 atm versus 150 atm, respectively. Countering the reduced P_{CO₂} for wollastonite, however, is its higher R_{CO₂} relative to forsterite. Because Ca is a much heavier element than Mg, the Ca-bearing silicates have a lower molar concentration of cations suitable for carbonation, and thus a higher R_{CO₂}. Both these factors have a significant impact on the process economics, which are discussed in greater detail in a later section.

Antigorite serpentine has the second lowest R_{CO₂} and the highest R_X of the minerals investigated. However, a heat pretreatment stage was necessary to achieve this degree of reactivity. Lizardite serpentine underwent an identical heat treatment stage to achieve the reported R_X,

although to less effect. The lower reactivity of the non-heat treated hydrated magnesium silicates is evident in the R_X of 15% reported for talc. Heat treatment proved an effective activation methodology for the hydrated minerals. However, as with the ultra-fine grinding used to activate olivine and wollastonite, heat treatment has a significant impact on the process economics and CO₂ balance.

Finally, the mafic rocks and/or minerals, including basalt, which is comprised in part of varying concentrations of anorthite, augite, magnetite, and olivine, all tended to exhibit the lowest R_X and the highest R_{CO₂}. The anorthite and augite tests included the ultra-fine grinding stage, but were conducted for longer carbonation times (6 hours) than the standard 1 hour carbonation time, thus the R_X for 1 hour for both would be lower than shown. Although the fayalite and magnetite tests were also conducted for 6 hours rather than the standard time, their R_X are believed to be comparable to the others because neither underwent the ultra-fine grinding stage.

MINERAL AVAILABILITY

Ultramafic Mineral Carbonation Regions

The ultramafic minerals investigated for mineral carbonation generally occur within large ophiolite complexes that are described as remnants of oceanic crust that have been compressed and folded along convergent continental margins. In North America, these ultramafic belts occur along both coasts, rather than the interior, which places limitations on the application of the mineral carbonation technology. The large tonnage of ore required for mineral sequestration makes it necessary to locate the mineral carbonation plant at the mine mouth, rather than at the CO₂ point source. As part of the mineral carbonation studies conducted at ARC, an evaluation of the scale of major CO₂ point sources and

their proximity to the potential mineral sources was conducted, resulting in the identification of 7 primary ultramafic mineral carbonation regions within the conterminous U.S. (Figure 1).



Figure 1. Ultramafic mineral carbonation regions.

Coal Consumption and Ore Tonnage To determine the potential scale for mineral sequestration, it was necessary to derive the total CO₂ point source emissions within a specified distance of the mineral sources within these 7 regions. To simplify this determination, CO₂ point sources were limited to coal-fired power plants that occur within 100- and 200-mile radii of the geographic center of the specific mining district or mineral deposit. Total CO₂ emissions were calculated from total regional coal consumption derived from Platts (2001), and carbon content of the coal used in that region after Babcock & Wilcox (1998). Assumptions for coal use by region include sub-bituminous/lignite Washington coal in Region 1, sub-bituminous Wyoming coal in regions 2 and 3, Texas lignite in region 4, and bituminous Pennsylvania coal in regions 5-7 (Table II). The total calculated CO₂ emissions for all 7 regions (604 Mt) represents ~30% of the total annual CO₂ emissions from U.S. coal-fired power plants, as reported by the EIA (2003).

Total ore demand in Table II was calculated assuming sequestration of 100% of the CO₂ emissions in each region, at the R_{CO₂} of the various mineral reactants, and the demonstrated extent of reaction (R_X). Experimental results were used for the latter at two levels of mineral pretreatment. Standard pretreatment for all minerals is defined as size reduction to 80% minus 400 mesh (37 μm). Activated pretreatment is specific to the mineral type: olivine and wollastonite were mechanically activated by the addition of an ultra-fine grinding stage; serpentine minerals were activated by the addition of a heat-treatment stage. The impact of the mineral pretreatment operations is dramatic, reducing the total ore tonnage by over 75%. However, as stated previously, these activation steps also impact process economics and the CO₂ balance. These latter two factors are discussed further in later sections.

Ultramafic Mineral Resources The regional ore demand totals included in Table II are very large, even for the activated mineral reactants. However, with two exceptions, the ultramafic mineral resources far exceed these demands. Roskill (1990) reported reserves of 1.8 Gt of unaltered dunite (>90% olivine) at the Twin Sisters deposit in NW Washington. This represents a 33-year supply for current Region 1 CO₂ emissions.

Coleman and Irwin (1977) and Goff et al. (1997) described the vast belts of serpentine in SW Oregon and the California Coast Ranges, which dwarf the annual estimated ore demands for both Regions 2 and 3. Less certain is the availability of serpentine from the Llano Uplift to meet the estimated ore demand of ~200-400 Mt/year for mineral sequestration in Region 4. A resource of over 1 Gt of serpentine is inferred after Barnes et al. (1950), which may be a 5-10 year supply at full-scale mineral sequestration. In contrast, the serpentine resource in Region 6, the State Line district along the Maryland-Pennsylvania border, is vast, as described by Pearre and Heyl (1960). However, the 300-600 Mt/year ore demand would require 20-40 50-kt/day open pit mines.

Hunter (1941) provided a detailed description of the olivine deposits in western North Carolina, and Roskill (1990) reported ~200 Mt of reserves. These reserve estimates indicate that the olivine supply in Region 5 could meet the ore demand for only 1-2 years, assuming ~120 Mt/year within the more limited 100-mile radius. Serpentine resources would have to substitute for olivine in Region 5. Virta (2001) reported wollastonite reserves in Region 7 at ~14 Mt, roughly a 6-month supply for the 100-mile radius ore demand. Alternatives to wollastonite would be needed, although increased demand could spur exploration that might extend the wollastonite supply.

Mafic Mineral Carbonation Regions

The most likely targets for mafic mineral exploitation are the three massive flood basalt provinces that occur within the conterminous U.S. (Figure 2).



Figure 2. Mafic mineral carbonation regions.

Table II. Annual coal consumption, CO₂ emissions, and ore demand by ultramafic mineral carbonation region.

| Region | Mining district/deposit | Mineral | R _{CO2} | R _x , % | | Radius, miles | Coal, Mt | C, wt pct | CO ₂ , Mt | Ore, Mt | |
|--------|-----------------------------|-------------------------|------------------|--------------------|------|----------------|----------|-----------|----------------------|---------|------|
| | | | | Std. | Act. | | | | | Std. | Act. |
| 1 | Twins Sisters, WA | Olivine | 1.8 | 61 | 81 | 100 100-200 | 5 | 70 | 13 | 38 | 29 |
| | | | | | | | 2 | 70 | 5 | 15 | 11 |
| 2 | Trinity-Siskyou Mtn, CA-OR | Serpentine (lizardite) | 2.5 | 9 | 40 | 100 100-200 | 4 | 70 | 10 | 303 | 64 |
| | | | | | | | 0 | 70 | 0 | 0 | 0 |
| 3 | Coast Range, Southern CA | Serpentine (lizardite) | 2.5 | 9 | 36 | 100 100-200 | 4 | 70 | 10 | 303 | 71 |
| | | | | | | | 0 | 70 | 0 | 0 | 0 |
| 4 | Llano Uplift, TX | Serpentine (lizardite) | 2.5 | 9 | 40 | 100 100-200 | 13 | 63 | 30 | 888 | 187 |
| | | | | | | | 18 | 63 | 42 | 1229 | 259 |
| 5 | Asheville, NC | Olivine | 1.8 | 61 | 81 | 100 100-200 | 20 | 74 | 54 | 160 | 121 |
| | | | | | | | 49 | 74 | 133 | 392 | 295 |
| 6 | State Line, MD-PA | Serpentine (antigorite) | 2.1 | 12 | 92 | 100 100-200 | 39 | 74 | 106 | 1822 | 242 |
| | | | | | | | 46 | 74 | 125 | 2149 | 285 |
| 7 | Willsboro, NY | Wollastonite | 2.8 | 43 | 82 | 100 100-200 | 4 | 74 | 11 | 70 | 37 |
| | | | | | | | 24 | 74 | 65 | 422 | 222 |
| Total | Region 1-7, ultramafic ores | | | | | | 228 | | 604 | 7790 | 1823 |

These flood basalt provinces contain vast amounts of material for mineral sequestration, although experimental studies indicate that reaction efficiencies are low and R_{CO2} high compared to the ultramafic minerals (Table I). Mafic regions 8 and 10 overlap ultramafic regions 1 and 6, respectively. The CO₂ emissions and ore demand totals were calculated separately, but by the same methods, with the results included in Table III.

The Columbia River Basalt Group (CRBG) of Region 8 has been described by Reidel et al. (1989), among other authors. The CRBG covers over 200,000 km² at an average thickness of 1 km. Green (1972) described the geology of the Keweenaw Rift System Basalts (KRSB) in Region 9, while Olsen et al. (1996) provided similar discussion of the Newark Basin Basalts (NBB) of Region

10. In each case, the tremendous tonnages required for *ex situ* mineral sequestration and the layered structure of each flood basalt province suggest they may hold greater promise for *in situ* mineral sequestration rather than as sources of mafic mineral reactants for the *ex situ* process. Reidel et al. (2002) reported on the potential for natural gas storage within anticlinal structures in the CRBG and speculated on the potential for CO₂ injection into deep saline aquifers hosted by the CRBG. Initial laboratory pressure-leach studies conducted at ARC on core from the CRBG were reported by O'Connor et al. (2003). The favorable basalt mineralogy for mineral carbonation could make these flood basalt provinces attractive targets for geological sequestration.

Table III. Annual coal consumption, CO₂ emissions, and ore demand by mafic mineral carbonation region

| Region | Mining district/deposit | Mineral | R _{CO2} | R _x , % | Radius, miles | Coal, Mt | C, wt pct | CO ₂ , Mt | Ore, Mt |
|--------|-------------------------|---------|------------------|--------------------|----------------|----------|-----------|----------------------|---------|
| 8 | CRBG, WA-OR | Basalt | 4.9 | 15 | 100 100-200 | 2 | 70 | 5 | 170 |
| | | | | | | 5 | 70 | 13 | 420 |
| 9 | KRSB, MN-WI-IA | Basalt | 4.9 | 15 | 100 100-200 | 13 | 69 | 33 | 8100 |
| | | | | | | 18 | 69 | 46 | 1500 |
| 10 | NBB, NJ-NY-PA | Basalt | 4.9 | 15 | 100 100-200 | 23 | 74 | 62 | 2000 |
| | | | | | | 34 | 74 | 92 | 3000 |
| Total | Region 8-10, mafic ores | | | | | 95 | | 251 | 15200 |

MINERAL PRETREATMENT

Activation of the mineral reactants has been achieved by both thermal and mechanical means, although the mechanism for this activation is not clearly understood. Because most mineral dissolution reactions are surface controlled, it is possible that the two pretreatment methods proved successful primarily due to increased surface area. Mechanical pretreatment reduces the mean

particle size of the minerals, while thermal pretreatment removes chemically-bound water, which may increase the porosity and the resulting surface area. Zhang et al. (1996) provided some discussion of the enhancement of Mg silicate solubility by mechanical means, while McKelvy et al. (2002) and Chizmeshya et al. (2002) described thermal activation and computational modeling studies, respectively, conducted at Arizona State University, a collaborating laboratory with ARC. All

suggest that the activation is due to destruction or disordering of the mineral lattice. It is likely that both phenomena are responsible to some degree for the improvements in mineral reactivity achieved by pretreatment. However, because the energy penalty necessary to achieve such activation is most critical to the viability of any mineral-carbonation process, the following discussion focuses on the energy consumption for the various mineral pretreatment options, rather than the root causes for enhanced reactivity.

Mechanical Activation

Mechanical activation was investigated by use of conventional rod and ball milling techniques, as well as ultra-fine grinding using a scalable stirred-media detritor (SMD) mill. The Work Index (grinding energy) necessary for specific size reduction was calculated for olivine and the two serpentine minerals, using data derived from pilot-scale comminution tests conducted on the ores and the formula described by Bond (1952). Energy consumption for ultra-fine grinding was determined by direct measurement from the SMD mill. Four test series were conducted on the primary mineral reactants to evaluate the sensitivity of mineral reactivity (R_x) to grinding energy (Figure 3).

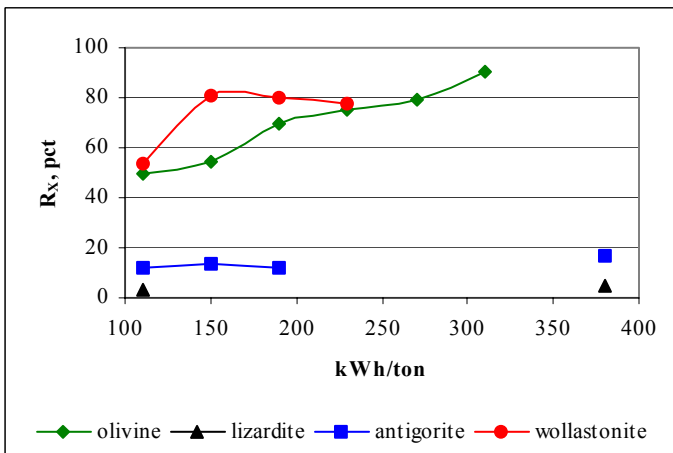


Figure 3. Grinding energy versus R_x .

The carbonation test conditions varied by mineral, using the best demonstrated reaction parameters: 1 hour duration (all minerals); 185°C (olivine), 155°C (serpentines), 200°C (wollastonite); P_{CO_2} of 150 atm (olivine and serpentines), 40 atm (wollastonite); carrier solution of 1 M NaCl, 0.64 M $NaHCO_3$ (olivine and serpentines), distilled water (wollastonite). While olivine showed a nearly linear relationship between mechanical energy input and R_x , wollastonite activation peaked at a much lower energy input, with no gain at higher energies. In contrast, both serpentine minerals show virtually no increase in R_x at energies up to nearly 400 kWh/ton. Additional studies using a laboratory-scale attrition-grinding mill showed significant activation of the serpentines, but the estimated energy consumption was

extremely high, and activation of serpentine by mechanical means alone appears impractical.

The relationship between particle size and surface area versus mechanical energy input was also examined for the olivine ground products (Figure 4). Particle size is represented by the D_{50} (50% finer than specified diameter) as determined by an X-ray absorption sedimentation method. Not surprising is the fact that olivine particle size decreases while reactivity increases with increasing grinding energy. Surface area measurements by BET N_2 adsorption increase from 2.6 to 10.2 m^2/g over this same series. Because all carbonation tests were conducted for 1 hour, reaction rates cannot be derived from these data, but it is likely that the increased surface area accelerated the dissolution rate of the mineral, leading to further extent of reaction within the 1-hour test time.

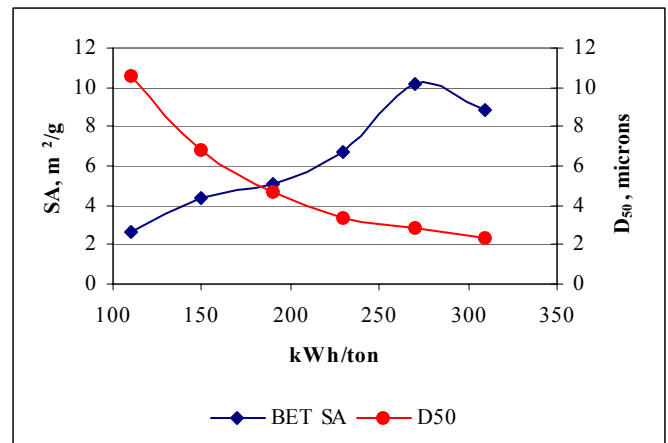


Figure 4. Olivine grinding energy versus particle size and surface area.

Thermal Activation

Thermal activation of the hydrated Mg-silicate species was accomplished by the addition of a heat treatment stage in the mineral pretreatment process. An effective heat treatment methodology was developed experimentally and confirmed by differential thermal analysis and thermal gravimetric analysis (DTA/TGA) of the antigorite serpentine ore sample (Figure 5).

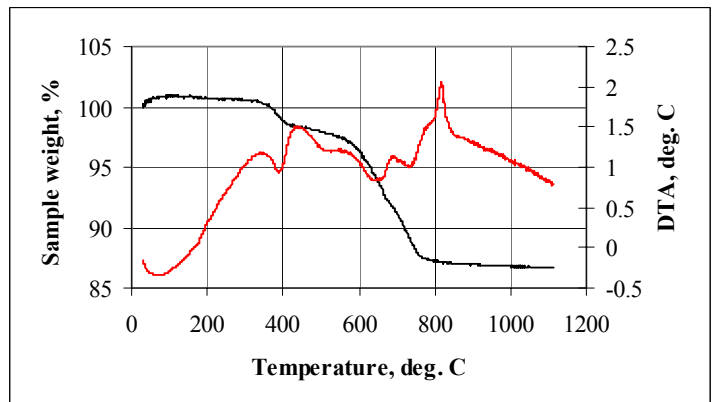


Figure 5. DTA (red) & TGA (black) for antigorite

The most effective heat-treatment temperature determined experimentally was approximately 630°C. This is reflected in the TGA plot, which shows the most significant weight loss, due to dehydroxylation or removal of the chemically-bound water, initiating at about 600°C. The DTA plot shows an endotherm in this temperature range centered on approximately 650°C, which corroborates the experimental data derived from bulk heat treatment of the ore. A second endotherm evident on the DTA plot occurs at about 390°C, coinciding with a weight loss of roughly 2% based on the TGA. This may be indicative of brucite [Mg(OH)₂] dehydroxylation, which occurs at roughly 375°C. X-ray diffraction (XRD) analysis of the same sample identified brucite as a minor phase (1-10%). DTA/TGA of the lizardite samples showed no similar weight loss or endotherm around 400°C, suggesting that brucite is absent from those ores. Because Mg-hydroxide species are far more reactive than Mg silicate, the presence of brucite in the antigorite sample may help explain the higher R_x achieved for that serpentine compared to the lizardite variety.

A great deal of study has focused on serpentine activation, both recently within the DOE Mineral Carbonation Study Group, and prior to the current research. Barnes et al. (1950) described extensive studies on the utilization and heat activation of Texas serpentine. Zhang et al. (1997) reported on the enhancement of acid extraction of Mg and Si from serpentine by mechanochemical treatment, although the 6-hour grinding times utilized likely make the methodology extremely energy-intensive. From a process standpoint, the energy consumption required for activation is more significant than the methodologies themselves, which led to an effort to determine the relative energies for thermal activation of the serpentine minerals used in the current study.

The theoretical energy required for the heat activation process must include the energy to heat the mineral to the specified temperature and the enthalpy of dehydroxylation. The latter includes the energy to decompose the serpentine, removing the hydroxyl molecule and producing a pseudo-amorphous silicate phase. Thermodynamic data reported by King et al. (1967) was used to calculate the effective heat capacities at temperature for antigorite serpentine. The theoretical energy required to heating the mineral to the specified temperature was calculated by equation 8.

$$Q = C_p \Delta T \quad \text{Eq. 8}$$

Where:

Q = heat, cal/mol

C_p = cal/K•mol @ temperature T₁, (K)

ΔT = T₁ – T₀ (298K)

Quantitative DTA analysis was utilized to determine the dehydroxylation energies (E_d) for antigorite and lizardite

serpentine, which were reported by Govier and Arnold (2004) to be approximately 95 and 131 kJ/mol, respectively. Combining the C_p data derived for antigorite serpentine coupled with these mineral-specific E_d values results in the total theoretical energy requirement for the heat-activation process. For example, heat treatment of the serpentine at 630°C (C_p = 89.26 cal/K mol) requires 206 kW•h/ton to heat the mineral, while dehydroxylation of the antigorite and lizardite requires an additional 87 and 120 kW•h/ton, respectively. Total energy consumption for the heat treatment process is thus 293 and 326 kW•h/ton, for antigorite and lizardite, respectively.

A series of heat treatment tests was conducted over a range of 200-1,000°C at 200°C intervals to evaluate the effect of heat-treatment temperature on antigorite serpentine reactivity. The reported energy values for the heat-treatment process represent the thermal energies required at each temperature as calculated by the method described above (Figure 6). The energies at the 200°C and 400°C heat treatment temperatures do not include the E_d because dehydroxylation does not occur at

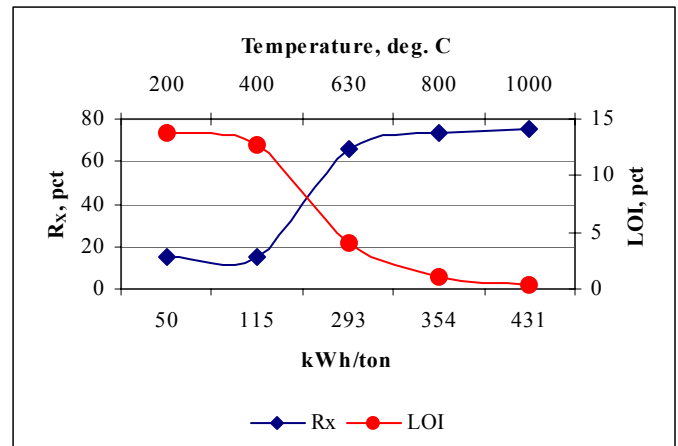


Figure 6. Antigorite heat treatment energy versus R_x.

temperatures below approximately 600°C.

The Loss-on-Ignition (LOI) curve was added to Figure 6 to emphasize the relationship between carbonation reactivity and effective removal of bound water. The LOI continues to decrease at temperatures above 630°C, although R_x increases only slightly, thus the added energy is not considered cost-effective. Barnes et al. (1950) identified an effective zone for activation that ranges from roughly 600-725°C, distinguished by an amorphous XRD pattern of the activated serpentine. McKelvy et al. (2001) described a meta-stable serpentine phase that forms in roughly the same temperature range, and suggested that heating above 800°C is undesirable, because this leads to a phase transformation to the non-hydrated Mg-silicate phases, forsterite and enstatite. This phase transformation is marked by an exotherm at just over 800°C (Figure 5).

Energy Consumption

Using the energy data compiled during the mechanical and thermal activation studies, a compilation of comparative energy consumption values was prepared for each of the 7 ultramafic mineral carbonation regions (Table IV). The feed material histories are summarized in the first three columns of the table, with a code specific to each material included in column 4. This code is used in subsequent tables to conserve space. The rest of the table includes the energy consumption values determined for the various mineral pretreatment methodologies by stage.

For example, crushing energy for all materials is estimated at 2 kW•h/ton, based on mining cost data produced by the U.S. Bureau of Mines (1987). Ore grade is assumed to be 100% for the Twin Sisters olivine and all serpentine mineral districts (Regions 1-4, 6), based on first-hand observation of several of the mining operations,

which are essentially open-pit quarries that require no concentration steps. However, laboratory analysis of olivine samples collected from the Asheville Mining District (Region 5) identified alteration minerals, serpentine and talc, with an estimated ore grade of 70% olivine. Bench-scale tests conducted on the Region 5 olivine ore indicated that gravity separation could be an effective beneficiation process, with an energy penalty of approximately 2 kW•h/ton. It is assumed that the beneficiation step would be conducted following the first grinding stage, which appears to provide sufficient liberation of the olivine from the alteration products based on the laboratory studies. Thus, the grinding energy for the stage 1 grind is based on the tonnage of raw ore processed, while subsequent pretreatment energies are based on processing the olivine concentrate.

Table IV. Energy consumption by feed material and specific pretreatment methodology.

| Feed Material History | | | | Pretreatment Energy Consumption, kW•h/ton | | | | | | |
|-----------------------|-------------------------------|--------------------------|------|---|-------|----------|---------|---------|----------------|-------|
| Region | Ore mineral & grade | Pretreatment methodology | Code | Crush. | Bene. | Grinding | | | Heat treatment | Total |
| | | | | | | Stage 1 | Stage 2 | Stage 3 | | |
| 1 | Olivine, 100% | Ball mill (-200 mesh) | 1A | 2 | | 11 | | | | 13 |
| | | Ball mill (-400 mesh) | 1B | 2 | | 11 | 70 | | | 83 |
| | | SMD mill | 1C | 2 | | 11 | 70 | 150 | | 233 |
| 2-4 | Serpentine, 100% (lizardite) | Ball mill (-200 mesh) | 2-4A | 2 | | 11 | | | | 13 |
| | | Heat treatment (-200) | 2-4B | 2 | | 11 | | | 326 | 339 |
| 5 | Olivine, 70% | Ball mill (-200 mesh) | 5A | 2 | 2 | 15 | | | | 19 |
| | | Ball mill (-400 mesh) | 5B | 2 | 2 | 15 | 70 | | | 89 |
| | | SMD mill | 5C | 2 | 2 | 15 | 70 | 150 | | 239 |
| 6 | Serpentine, 100% (antigorite) | Ball mill (-200 mesh) | 6A | 2 | | 11 | | | | 13 |
| | | Heat treatment (-200) | 6B | 2 | | 11 | | | 293 | 306 |
| | | Heat treatment (-400) | 6C | 2 | | 11 | 70 | | 293 | 376 |
| 7 | Wollastonite, 50% | Ball mill (-400 mesh) | 7A | 2 | 4 | 21 | 70 | | | 97 |
| | | SMD mill | 7B | 2 | 4 | 21 | 70 | 70 | | 167 |

Virta (2001) reported wollastonite grade in the Region 7 deposits at 40-60%. Information provided with samples from the largest wollastonite mining operation in Region 7 described a two-stage concentration process, including size separation to remove calcite and magnetic separation to remove garnet. The wollastonite ore grade was assumed to be 50% for the subject calculations, and a beneficiation energy penalty of 4 kW•h/ton was added to the overall pretreatment energy consumption figure. As with the Region 5 olivine beneficiation, the size and gravity separation steps would be conducted on the raw wollastonite ore following the first-stage grind, which increases the grinding energy for that stage accordingly, compared to the non-beneficiated ore materials. Subsequent pretreatment energies are based on processing the wollastonite concentrate.

This compilation was used to calculate the theoretical parasitic energy loss from the power plant, based on the measured mechanical/thermal activation energies and experimental carbonation data. The basis for this calculation was a 1 GW coal-fired power plant, burning coal with an as-fired heat value of 12,500 Btu/lb and

carbon content of 74%, at 35% plant efficiency. The CO₂ emissions of 25.4 kt/day were then used to calculate the daily ore requirement to sequester 100% of the CO₂ emissions at the R_{CO2} and demonstrated R_X of each mineral reactant in a single pass through the carbonation reactor. The results are included in Table V.

Table V. Parasitic energy loss by pretreatment.

| Feed Code | R _{CO2} | R _X , % | Ore/conc., kt/day | Pct total plant energy |
|-----------|------------------|--------------------|-------------------|------------------------|
| 1A | 1.8 | 16 | 286 | 15 |
| 1B | 1.8 | 61 | 75 | 26 |
| 1C | 1.8 | 81 | 56 | 55 |
| 2-4A | 2.5 | 9 | 706 | 37 |
| 2-4B | 2.5 | 40 | 158 | 222 |
| 5A | 1.8 | 16 | 286 | 22 |
| 5B | 1.8 | 61 | 75 | 28 |
| 5C | 1.8 | 81 | 56 | 56 |
| 6A | 2.1 | 12 | 445 | 24 |
| 6B | 2.1 | 62 | 86 | 110 |
| 6C | 2.1 | 92 | 58 | 90 |
| 7A | 2.8 | 43 | 165 | 67 |
| 7B | 2.8 | 82 | 87 | 61 |

While the daily ore requirements decrease dramatically with increased mineral activation, the coincident parasitic energy loss on the power plant becomes problematic. The latter is critical because it provides an estimate of the CO₂ balance, based on the pretreatment energies only. For example, the 15% of total plant energy necessary for pretreatment methodology 1A (minus 200-mesh Twin Sisters olivine) indicates that the CO₂ avoided is approximately 85% for that feed material at that degree of pretreatment. This assumes that the energy required for the pretreatment operation is generated by burning the same coal at the same efficiency as stated for the power plant. Adding the sequestration plant energy requirement decreases the CO₂ avoided even further. Parasitic energy losses exceeding unity (1.0) indicate that the CO₂ avoided is negative, meaning that more CO₂ is emitted by the pretreatment operation than is sequestered. These problems are most acute for the thermal-activation operations on the serpentine minerals, but the high energy consumption for the mechanical activation operations on the olivine and wollastonite minerals are also problematic.

The improved reactivity achieved by the additional pretreatment operations is negated for the most part by the higher energy demand. However, the higher ore requirements at the lower pretreatment energies require massive increases in mining output, exceeding the available resources in some regions. These calculations assume a single pass of the mineral through the carbonation plant; the successful addition of a recycle stream could reduce the virgin ore demand significantly. This issue is discussed further under the Process Development section later in this report.

Physical Properties

Several physical properties of the specific pretreatment products were measured for comparison. The results included in Table VI provide some insight into the mechanisms impacting the activation phenomena.

Table VI. Physical properties of the pretreatment products.

| Feed Code | D ₈₀ , μm | D ₅₀ , μm | BET SA, m ² /g |
|-----------|----------------------|----------------------|---------------------------|
| 1A | 75 | 20 | 5 |
| 1B | 37 | 14 | NA |
| 1C | 10 | 3 | 7 |
| 2-4A | 75 | 19 | 32 |
| 2-4B | NA | 22 | 11 |
| 5A | NA | NA | NA |
| 5B | NA | NA | NA |
| 5C | NA | NA | NA |
| 6A | 75 | 13 | 9 |
| 6B | NA | NA | NA |
| 6C | 37 | 17 | 19 |
| 7A | NA | NA | NA |
| 7B | NA | NA | NA |

The D₈₀ values correspond with the size reduction targets for the stage-1 grinding operations. The minus 200-mesh ball mill product from pretreatment methodology 1A represents material that is 80% finer than 75 μm, and so on. The further reduction in particle diameter with each succeeding stage of grinding is reflected in both the D₈₀ and D₅₀ values. Particle diameters below 10 μm may significantly reduce if not eliminate diffusion limitations at the mineral specific carbonation reaction conditions, while coincident increases in surface area improve the mineral dissolution kinetics. Both phenomena improve R_x, although at significant energy penalty, as specified in Table IV.

The heat-activation process on the serpentine minerals tended to increase the mean particle diameter for both minerals, but with opposite impacts on the surface areas. Lizardite (2-4B) surface area decreased by nearly 300% after heat treatment, while antigorite (6B and C) surface area increased by over 200%. These variations in surface area may help to explain the much higher reactivity of the heat-activated antigorite compared to that of the heat-activated lizardite. The reason for the variable surface areas after removal of the bound water is likely tied to the different lattice structures of the two minerals a discussion beyond the scope of this paper.

REACTION PARAMETRICS

Experimental Procedure and Apparatus

Series of laboratory experiments were conducted at ARC to define the optimum carbonation reaction conditions specific to each mineral investigated. Foremost in this process was the development of an effective experimental apparatus and procedure, both of which can have a significant impact on the R_x. For example, initial tests were conducted in a batch autoclave system with continuous agitation but did not include gas dispersion or a means to maintain constant P_{CO₂}. The stirred-tank-reactor (STR) was prepared for operation by the following procedure:

1. 100 g olivine weighed and placed in the STR;
2. 400 ml distilled water poured into the STR;
3. STR sealed, evacuated, weighed (tare weight), and placed into an ice bath;
4. liquid CO₂ introduced into the STR;
5. STR placed back on scale, weight of CO₂ determined;
6. pressure bled off while STR on scale until proper weight of CO₂ remained;
7. STR heated to final process P and T;
8. after specified test time, STR cooled, pressure bled off, slurry removed;
9. slurry filtered, solids dried, weighed, and sampled for analysis, solution sampled for analysis.

The proper weight of CO₂ was calculated in advance using the compressibility factor equation of state (equation 9).

$$P\hat{V} = zRT \quad \text{Eq. 9}$$

Where:

P = pressure, atm

\hat{V} = molar volume, moles/liter

z = compressibility factor for CO₂

R = gas constant, liter•atm•mole⁻¹•K⁻¹

T = temperature, K

The CO₂ compressibility factor was initially interpolated from the available literature and then modified based on the empirical results. The solubility of CO₂ in water at the desired P-T conditions was also included in the final calculation.

This procedure was simplified dramatically by the development of a new batch autoclave system that included a CO₂ gas booster pump controlled by a pressure transducer on the autoclave (Figure 7).

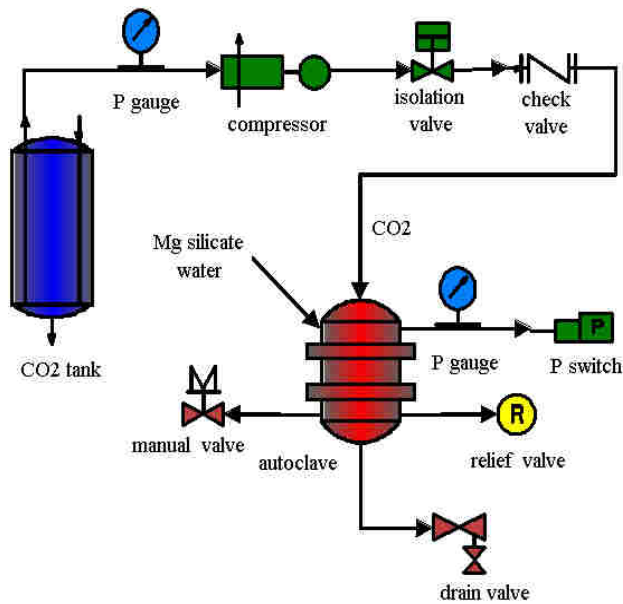


Figure 7. Schematic of laboratory apparatus.

All subsequent tests conducted in the new system followed a simplified test procedure. The pre- and post-test solids and solution handling procedures were not changed, but the inclusion of the gas booster pump permitted operation under relatively constant P_{CO_2} , which was not possible in the former system. This minimized the impact of decreasing P_{CO_2} due to carbonation and/or system leaks on the final R_X . In addition, the use of a gas-

dispersion agitator dramatically improved three-phase mixing in the reactor, which ultimately improved R_X without changing P and T conditions or residence time. The modified test procedure follows.

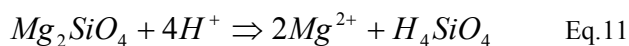
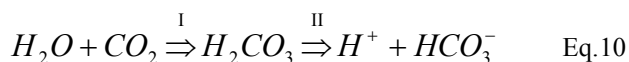
1. 167 g of mineral reactant and 950 g carrier solution (distilled water or bicarbonate/salt solution) poured into STR;
2. STR sealed, purged with CO₂;
3. STR heated to test T;
4. CO₂ injected to test P;
5. additional CO₂ injected as system pressure decreases due to reaction and/or leaks;
6. after specified test time, STR cooled, pressure bled off, slurry removed;
7. slurry filtered, solids dried, weighed, and sampled for analysis, solution sampled for analysis.

In the new system, the autoclave was sealed and purged with CO₂ following the addition of the slurry. This left a residual atmosphere of about 10 atm P_{CO_2} during the heat-up interval, which was standardized to 1 hour. To discern the extent of reaction that had occurred during the heat-up interval, zero-time tests were conducted for each mineral reactant. These tests were terminated once the system had reached the desired temperature, but prior to CO₂ injection to the final elevated pressure. Results showed that R_X was mineral-specific, being negligible for the olivine and non-heat-treated serpentine minerals, but much more significant for the wollastonite and heat-treated serpentines.

The zero-time R_X measurements for the heat-treated antigorite, heat-treated lizardite, and wollastonite were roughly 18, 34, and 45 pct, respectively. The reported test times are designated only for time at the test P and T conditions; the 1-hour heat-up times were neglected. The results from the zero-time tests indicate that the true test times should account for the heat-up interval, at least for the more highly reactive mineral species. However, for the purpose of this report, it was assumed that the highly reactive portion of these mineral species would also react within the 1-hour test time at the final P and T conditions if the system permitted introduction of the slurry into the reactor at these conditions. Perhaps more significant is the relatively high R_X for these activated minerals at much-reduced P_{CO_2} and reduced temperature during the heat-up interval.

Carbonation Carrier Solution

Carbonic Acid System: The original aqueous mineral carbonation process investigated at ARC used distilled water (pH = 5.8) as the carbonation carrier solution, and was thus considered the carbonic-acid route. Hem (1985) pointed out that, while carbonic acid (H_2CO_3) is conventionally used to represent all the dissolved undissociated CO_2 in natural waters, only about 0.01 pct of the dissolved CO_2 is actually present in this form. Thus, the H_2CO_3 convention used to describe the process has no practical effect on the results. These initial tests were exploratory in nature and intended to provide a baseline regarding the impact of solution chemistry on the overall mineral-carbonation process. One possible reaction sequence for the carbonic-acid route includes several simultaneous reactions. In this sequence, bicarbonate formation within the solution occurs by hydration of CO_2 to form carbonic acid, which dissociates to the separate hydrogen and bicarbonate ions (equation 10).



Mineral hydrolysis liberates Mg^{2+} cations from the forsterite olivine, with co-production of silicic acid and/or free silica and water (equation 11). Carbonation of the Mg^{2+} cations would then occur by reaction with the HCO_3^- to produce the solid carbonate and additional H^+ for further mineral hydrolysis (equation 12). Regarding equation 10, Nguyen et al. (1984) stated that while equilibrium with the bicarbonate ion is very fast (reaction II), the formation of carbonic acid (reaction I) is the rate-determining step. This is likely due to the slow dissolution rate of CO_2 in water, as described by Sherwood and Pigford (1952). Reaction I may also be rate-limiting for the overall mineral carbonation process in the carbonic-acid system, although forsterite dissolution and magnesite precipitation kinetics also play significant roles. The positive impact of the modified experimental apparatus, which included gas dispersion for improved three-phase mixing, on the overall reaction efficiency is likely due in part to improved rates for equation 10. A complete discussion of the CO_2 hydration reaction kinetics is beyond the scope of this paper. However, it is readily seen that finding a means to facilitate aqueous bicarbonate formation would help overcome this rate-limiting step.

Bicarbonate System: Based on the results from the initial test series, it was theorized that solution pH plays a conflicting role in the two-stage reaction process. While acidic solutions should favor mineral hydrolysis and improve silicate dissolution rates, carbonate precipitation likely requires alkaline solutions. Thus, a buffered

solution chemistry was formulated that permits simultaneous silicate dissolution and carbonate precipitation. In this new system, $NaHCO_3$ was added to the solution, serving the dual purpose of modifying the solution to slightly alkaline pH while acting as an effective CO_2 carrier. The impact of this addition was immediately apparent, reducing the required residence times to achieve an R_X of approximately 80% from 24 to 6 hours, all other carbonation conditions being constant. One interpretation of the modified reaction sequence includes direct reaction between the forsterite olivine and bicarbonate ion (equation 13), followed by immediate bicarbonate regeneration due to reaction of CO_2 with the hydroxide ion (equation 14).



The actual ionic species present at the carbonation P and T conditions are not known, thus speculation on whether OH^- could exist in this system is tenuous, but at the pH of the buffered solution (~7.9), typical silicate hydrolysis does not occur. Characterization of the reaction products tends to support this assertion, with identification of a silica-rich outer layer on the coarser, partially-reacted silicate grains. These zones are depleted of Mg^{2+} cations, suggesting that the cation is mobilized rather than the silica, the latter being the expected path for typical mineral hydrolysis.

Regardless of the actual reaction pathway, the bicarbonate carrier solution was refined experimentally by using various concentrations of $NaHCO_3$, with and without $NaCl$. The $NaCl$ addition improved R_X at constant $NaHCO_3$ concentration and P and T. The additional Na^+ ions may modify the surface charge of the silicate particles, aiding in the ion exchange at the solid/liquid interface. The Cl^- ions may provide a means to complex the Mg^{2+} cations, at least temporarily, increasing the Mg^{2+} solubility. The combination of $NaHCO_3$ and $NaCl$ was found to be most effective, with the optimum concentrations based on the demands of an industrial process utilizing solution recycle. The final combination of 0.64 M $NaHCO_3$ and 1 M $NaCl$ is the maximum solubility of the two compounds in water at ambient conditions. Although higher concentrations were demonstrated to be technically feasible at the elevated P and T utilized, excessive losses of the dissolved salts to the solids would likely occur during post-carbonation gas/solid/liquid separation. The latter must occur at temperatures well below 100°C to permit recycle of a water-vapor-free CO_2 stream, which would lead to precipitation of some portion of the salts. Conservative solution concentrations were used in these tests, recognizing that room was available for further refinement of the carrier solution.

Carrier Solution pH: To further investigate the impact of pH on the complex mineral-dissolution and carbonate-precipitation sequence, a series of tests was conducted over a pH range of 2.4 to 12.3. The pre- and post-test solution pH and descriptions of the various carrier solutions for several tests are included in Table VII.

Table VII. Carrier solution, pH and R_X ¹.

| Solution pH | | Carrier solution | R_X |
|-------------|-------|---|-------|
| Initial | Final | | |
| 2.36 | 7.08 | 1 M NaCl (1 ml 100 g/L HCl) | 45 |
| 5.89 | 7.22 | 1 M NaCl | 47 |
| 7.88 | 7.99 | 0.64 M NaHCO ₃ , 1 M NaCl | 83 |
| 9.49 | 8.04 | 0.25 M NaHCO ₃ , 0.25 M Na ₂ CO ₃ , 1 M NaCl | 80 |
| 11.02 | 7.79 | 0.5 M Na ₂ CO ₃ , 1 M NaCl | 79 |
| 12.25 | 7.26 | 4.5 g/L NaOH, 1 M NaCl | 49 |

¹ Test conditions: heat treated antigorite serpentine; T = 185°C, pCO₂ = 115 atm, 3 hours.

In each case, solution pH migrated toward that of the buffered solution (initial pH = 7.88). Solutions with the most extreme initial pH achieved the lowest R_X . In the current system, HCO₃⁻ appears to be the dominant dissolved CO₂ species. The essentially infinite supply of CO₂ made available to the solution by continuous three-phase mixing in the reactor apparently makes pH migration from the extremes unavoidable. Hem (1985) described the relationships among the dissolved CO₂ species and pH in a CO₂ species distribution diagram (Figure 8). Superimposed on the diagram are data points corresponding with the final solution pH versus R_X for the tests reported in Table VII. The combined diagram illustrates that in all cases the final solutions fall within the HCO₃⁻ region, and suggests that R_X is highest for solutions with the highest HCO₃⁻ concentration. For example, a final solution with a pH = 8.0 is comprised of roughly 2% H₂CO₃ (aq) [CO₂ (aq)] and 98% HCO₃⁻. Because reagent make-up to maintain a more acidic or alkaline starting solution would become problematic, any benefit due to enhanced mineral dissolution rate by use of the more aggressive solution is lost.

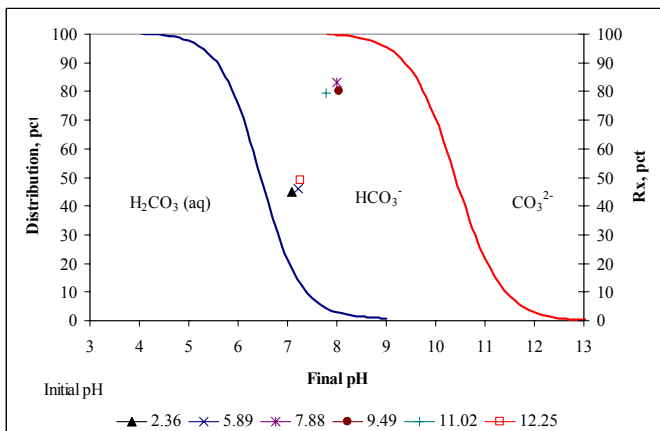
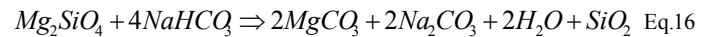


Figure 8. Carbon dioxide species distribution diagram.

Thermodynamics: To better understand the improved overall carbonation rate in the bicarbonate system, the theoretical free energies of formation for a set of stoichiometric carbonation equations were determined. These equations represent the combined mineral dissolution and carbonate precipitation reactions in the carbonic-acid (equation 15) and bicarbonate (equation 16) systems. Equation 17 shows regeneration of the NaHCO₃ by absorption of CO₂ and water.



The theoretical free energies of formation were determined at 1 atm CO₂ and various temperatures using HSC thermodynamics software (1995), with the respective trends included in Figure 9. The ΔG_f for equation 16 becomes negative at roughly 150°C, which corresponds well with the favored temperature range (~150-200°C) identified for Mg-silicate carbonation. In contrast, the ΔG_f for equation 15 becomes positive at precisely the same temperature, which may help explain the dramatic improvement in overall carbonation rate in the bicarbonate-based system.

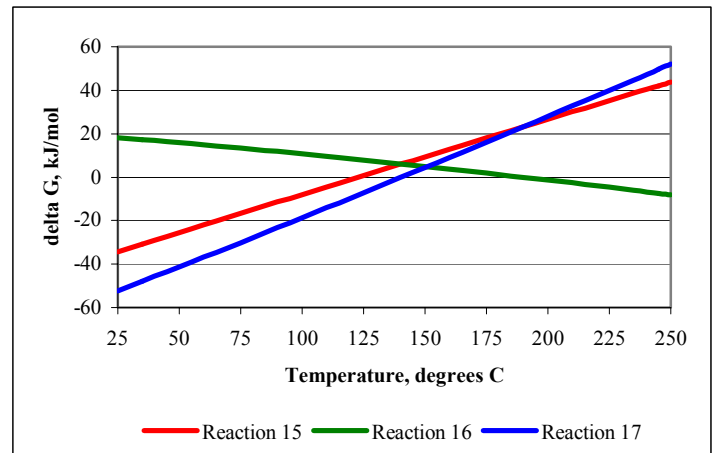


Figure 9. Gibbs free energy of formation for a selection of carbonation reactions, @ 1 atm CO₂.

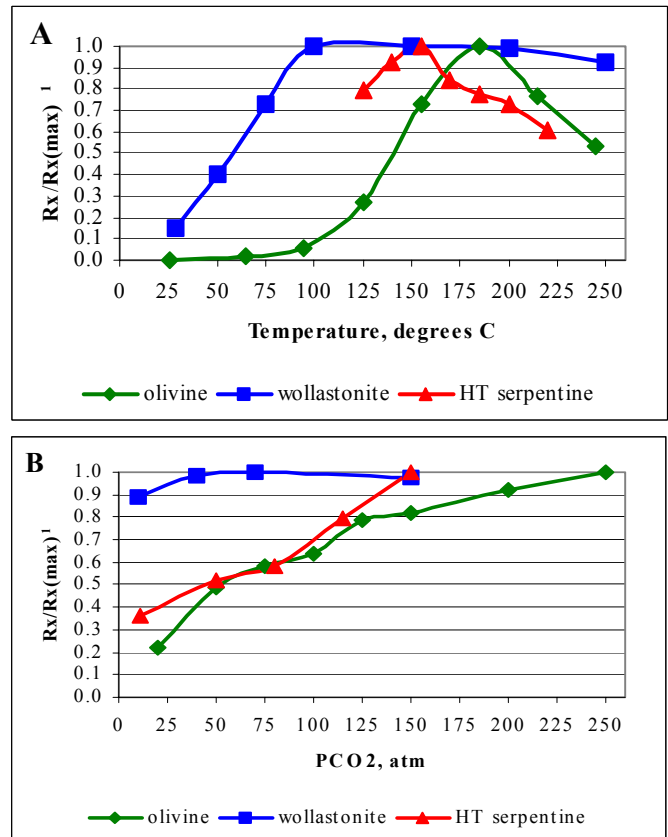
Although both equation 15 and equation 17 exhibit positive and thus unfavorable ΔG_f in the favored carbonation temperature range, it is likely that elevated P_{CO₂} drives those reactions to the right. Thus, the P and T conditions used for Mg silicate carbonation may represent a favorable thermodynamic window for both the mineral carbonation and bicarbonate regeneration reactions, particularly in the bicarbonate system.

Ca-Silicate Carrier Solution: The discussion of carrier solutions thus far has referred exclusively to Mg-silicate carbonation. Tests using the Ca-silicate, wollastonite, quickly revealed a significant change in carrier-solution requirements, compared to those for the Mg-silicates. Experimental results demonstrated that Ca-silicate carbonation was not as sensitive to solution dynamics, with equivalent R_X achieved in both the carbonic acid and bicarbonate systems. This may be indicative of a relatively higher solubility for wollastonite compared to the Mg silicates used, but is more likely due to the much higher precipitation rate for calcium carbonate compared to magnesium carbonate. Pokrovsky et al. (1999) reported that magnesite ($MgCO_3$) precipitation rates are at least 4 orders of magnitude lower than those of calcite ($CaCO_3$). Thus, wollastonite carbonation may not require the ionic concentrations or CO_2 activity necessary for Mg-silicate carbonation.

Carbonation Temperature and Pressure

To better define the optimum carbonation conditions, several test series were conducted to investigate carbonation sensitivity to both temperature and P_{CO_2} . Each test series was conducted at a mineral-specific set of constant carbonation conditions, while varying the critical variable of temperature or pressure, respectively. Discrepancies in the carbonation conditions were ignored where they do not impact the relative trends. For example, the carbonation tests were conducted for 3 hours on the heat-treated (HT) antigorite serpentine, but for only 1 hour on the olivine and wollastonite; this was necessary to achieve distinguishable reaction efficiencies at the lower P and T conditions. The relative R_X trends exhibited for each mineral series are most critical, rather than comparisons of the maximum achieved R_X between minerals. Thus, the R_X values were normalized by dividing the measured R_X by the maximum R_X achieved in that series, to eliminate mineral-specific variations due in part to differing pretreatment methodologies, carbonation carrier solutions, and/or P and T. The normalized carbonation temperature and P_{CO_2} sensitivity diagrams are included in Figures 10A and 10B.

Perhaps most striking about the sensitivity diagrams is the different trends exhibited by the Mg-silicate minerals compared to the Ca-silicate mineral. In Figure 10A, both the olivine and heat-treated serpentine show a sharp peak in R_X at specific carbonation temperatures, 185°C and 155°C, respectively. In contrast, the wollastonite R_X increases at a similar rate until a minimum threshold temperature (100°C) is reached, above which the R_X remains nearly constant over a broad temperature range. Because the carbonation process includes two distinct reactions, mineral dissolution followed by carbonate precipitation, temperature plays a complex role. Dissolution kinetics improve with increasing temperature, but carbonate precipitation is retarded at higher temperatures due to reduced CO_2 activity. Bischoff and



¹ $R_{X(max)}$ for each mineral was achieved at specific conditions used for each series, which were not optimized.

Figure 10A. Carbonation temperature sensitivity diagram.

Figure 10B. Carbonation P_{CO_2} sensitivity diagram.

Rosenbauer (1996) described a similar phenomenon regarding wallrock alteration in CO_2 -charged waters as the “unreactivity of CO_2 at higher temperatures.” The fact that the wollastonite is much less affected by changes in temperature is likely indicative of the much higher rate of calcite precipitation relative to magnesite.

Similarly, the mineral-specific trend plots in Figure 10B show that the Mg-silicate minerals exhibit a nearly linear increase in R_X with increasing P_{CO_2} , while the wollastonite appears nearly independent of P_{CO_2} above about 40 atm. These differences can again be traced to the much higher rate of calcite precipitation relative to magnesite, making wollastonite much less dependent on P_{CO_2} than the Mg-silicate minerals. These trends were inferred by the mineral-specific carrier solutions as well. The best R_X for the Mg silicates were achieved in the bicarbonate system, while those for wollastonite were achieved in the carbonic-acid system. Because the former contains dramatically higher concentrations of CO_2 relative to the latter, the improved R_X for Mg-silicate carbonation may suggest that CO_2 activity plays a role in the Mg-silicate mineral-dissolution reaction as well.

Optimized Carbonation Conditions

Based on the empirical data presented thus far, the optimum mineral-specific carbonation conditions were derived and are reported in Table IX. These conditions are meant to represent the best-demonstrated reaction parametric space to date and not to preclude future advancements. Process considerations were also used in the evaluation. For example, although olivine R_X increases with increasing P_{CO_2} , pressures above 150 atm were considered impractical, due to the limited improvement in R_X at higher P_{CO_2} . The highest R_X should be achieved at these conditions and depends on the mineral pretreatment intensity. Mineral activation by more aggressive pretreatment should improve absolute R_X at these optimum carbonation conditions.

Table IX. Optimum carbonation conditions, by mineral.

| Mineral | Carbonation conditions | | |
|---------------|------------------------|------------------|--------------------------------|
| | T, °C | P_{CO_2} , atm | Carrier solution |
| Olivine | 185 | 150 | 0.64 M $NaHCO_3$, 1 M NaCl |
| Wollastonite | 100 | 40 | Distilled water |
| HT serpentine | 155 | 115 | 0.64 M $NaHCO_3$, 1 M NaCl |

PROCESS DEVELOPMENT

Mineral Carbonation History

Lackner et al. (1997a,b, 1998) provided some of the earliest discussion of mineral sequestration of anthropogenic CO_2 emissions. Together with colleagues from the Los Alamos National Laboratory (LANL), he proposed the LANL aqueous process for mineral carbonation of serpentine ores. The LANL process is a derivation from an earlier technology developed during World War II by the Tennessee Valley Authority and U.S. Bureau of Mines for production of Mg metal from olivine. Houston and Rankin (1942) and Houston and Kerr (1945) described an HCl acid-leach process for Mg extraction, followed by electrolysis of the $MgCl_2$ leach product for metal recovery and acid regeneration. Silica gel formation during pH adjustment was recognized as a challenge to the process, which was otherwise technically feasible but not economically favored.

The LANL process substituted a complex $MgCl_2$ dehydration and crystallization operation for the electrolytic stage of the TVA/USBM process. The crystallized $MgCl_2$ is converted to $Mg(OH)_2$ during an acid recovery step, which is followed by carbonation of the $Mg(OH)_2$. Nilsen and Hundley (1999) conducted a preliminary feasibility study of the LANL process to quantify the energy-intensive dehydration and crystallization steps. Power requirements for the sequestration operation result in a negative CO_2 balance, such that CO_2 produced by generating the energy to run the process far exceeds the CO_2 sequestered by the process. These results led to investigation of the ARC

aqueous process as an alternative method for *ex situ* mineral carbonation.

Reactor Design

The ARC aqueous mineral-carbonation process has been demonstrated using a batch autoclave with continuous stirring and constant temperature and P_{CO_2} capability. An industrial-scale process clearly requires continuous processing, and the elevated P and T conditions make reactor design a critical issue. Because required wall thickness for a pressure vessel is directly related to pressure and diameter, large-scale conventional autoclave reactors operating at 150 atm would be extremely thick-walled and very capital intensive. An ideal reactor design would entail minimal diameter to limit wall thickness without limiting scale. A continuous pipeline reactor meets these criteria for the current aqueous mineral carbonation process; a conceptualized view of such a reactor is shown in Figure 11.

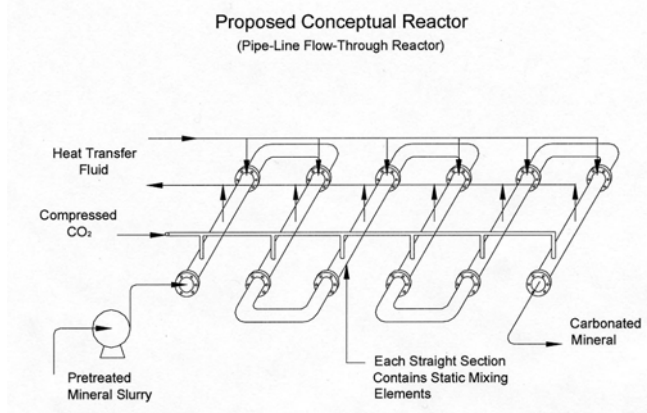


Figure 11. Conceptual pipeline reactor.

As a proof-of-concept of the pipeline reactor, a loop reactor was conceived that would permit operation in the pipeline design without the need to build a full-scale reactor. Figure 12 shows the loop reactor constructed at ARC prior to installation of insulation.



Figure 12. Laboratory-scale flow loop reactor.

Slurry is circulated for specified residence times while critical performance parameters such as three-phase mixing with static mixers, fluid flow at supercritical CO₂ pressures, and pre- and post-test slurry injection and removal are evaluated. Engineering data acquired by operation of the flow-loop reactor may be used for the design and construction of a pilot-scale continuous pipeline reactor. However, before any discussion of construction of a second-generation pipeline reactor was warranted, a feasibility study of the current aqueous mineral carbonation process was necessary.

Process Feasibility Study

The feasibility of mineral carbonation as a method for CO₂ storage has been the subject of several previous studies. The EIA (1999) commissioned an exhaustive study of several methods proposed by LANL, including the original LANL aqueous process, and several molten salt processes described by Wendt et al. (1998a,b,c). Sequestration costs were estimated at \$60-80 per ton CO₂ for the favored molten salt process, which is yet to be demonstrated, to over \$200 per ton CO₂ for the LANL aqueous process. Both methods were found to be currently untenable, due to the excessive energy demand for the aqueous process, and excessive chemical make-up volumes for the molten salt process. Energy demand for the former was determined by both the EIA study and by Nilsen and Hundley (1999) to be over 4 times the energy produced by the power plant for which the process was designed to accommodate. The latter was estimated to use nearly 1/3 of annual world HCl production for sequestration of 100% of the CO₂ emissions from a single 500-MW power station.

A second feasibility study was conducted by NEXANT (2000) for an anaerobic hydrogen/electric power generation plant with CO₂ disposal by mineral carbonation. This was the first study to include the ARC aqueous process for the mineral-carbonation step, in this case applied to serpentine carbonation. Sequestration costs were estimated at \$70 per ton CO₂, including a heat-activation step. The estimated energy demand for the heat-treatment step was much lower than that reported here, at 153 kW•h/ton compared to 293 kW•h/ton (antigorite) or 326 kW•h/ton (lizardite). The sequestration cost was calculated assuming a plant efficiency of 65% for the anaerobic hydrogen/electric power production technology, compared to a typical coal-fired power plant efficiency of 35%. Sequestration costs applied to conventional coal-fired technology were roughly \$130 per ton CO₂.

A third mineral carbonation feasibility study was commissioned by the National Energy Technology Laboratory (NETL) and completed by Lyons et al. (2003), using a preliminary process design and basis developed at ARC by Nilsen and Penner (2001). A steady-state simulation of the process was created in Aspen® process simulation software, from which capital- and operating-

cost estimates were generated. This study evaluated an olivine-based mineral-carbonation process scaled for the sequestration of 100% of the CO₂ emissions from a 1.3 GW coal-fired power plant. Olivine was selected as the mineral reactant in part to simplify the process by eliminating the heat-pretreatment stage. The process flow diagram is shown in Figure 13.

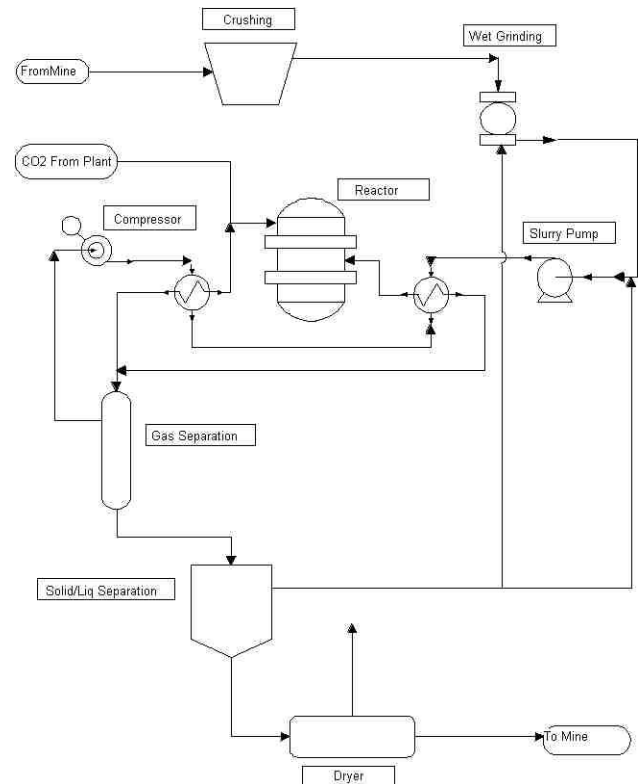


Figure 13. Aqueous mineral carbonation process

Because the proposed pipeline reactor design referred to above was unproven at the time, a conservative approach was adopted and conventional continuous-flow leach-type autoclave reactors were selected for the study (Figure 14).

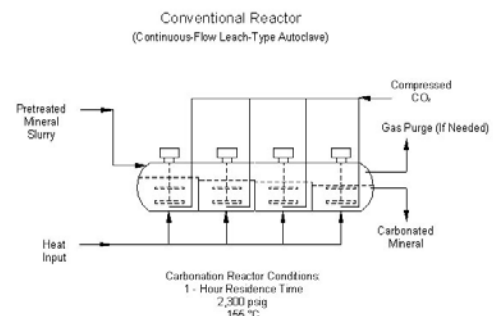


Figure 14. Conventional reactor design used in feasibility study.

The impact of the conventional reactor design on the process economics is significant. The design required 12-foot diameter vessels with 14-inch thick walls, which accounted for roughly 50% of total capital costs. Additional assumptions and selected bases for the feasibility study follow:

- Olivine is the mineral reactant, with an ore grade of 100% and MgO concentration of 49 wt pct;
- Olivine ore is ground to 80% minus 400 mesh (37 microns);
- 65% reaction efficiency (R_X) with each pass through the process;
- 60% of the unreacted olivine from the products is separated at 20 μm size and recycled;
- Twin Sisters olivine (Region 1) is utilized for the process, with the sequestration plant located next to the mine site;
- The mining operation is open pit, and the process products re-deposited in the depleted pits;
- CO_2 is transported to the plant via pipeline (CO_2 separation costs are not included in mineral sequestration cost estimates);
- Carbonation conditions include: 2 hour residence time; $T = 185^\circ\text{C}$; $P_{\text{CO}_2} = 150 \text{ atm}$; $P_{\text{H}_2\text{O}} = 6.5 \text{ atm}$; 30% solids; carrier solution = 0.64 M NaHCO_3 , 1 M NaCl .

The NETL study evaluated sequestration of approximately 1,100 tons of CO_2 per hour, requiring roughly 2,500 tons of virgin olivine ore plus an additional 800 tons of olivine from an unreacted product recycle loop every hour. Power requirements total 352 MW, with nearly 75% of the total power required for the ore-grinding operations. This power represents a 27% energy penalty on the power plant for which the sequestration operation was designed. Sensitivity analyses were conducted to evaluate the impact of reduced reactor residence time and P_{CO_2} on the overall sequestration cost and energy demand. These results were used to derive the carbonation costs for the alternative mineral feedstocks described in this report, as well as the overall carbonation costs and CO_2 balance by mineral-carbonation region.

Carbonation Costs

The final carbonation cost determined in the NETL feasibility study was \$69 per ton CO_2 sequestered for the baseline olivine process described above. This baseline process applies directly to ultramafic mineral carbonation in Region 1, as described in Table II. However, the R_X reported in the subject study were achieved in 1-hour reactor residence times rather than the 2-hour residence time assumed for the NETL study. Thus, the sequestration cost was lowered to \$54 per ton CO_2 , based on the reactor residence-time sensitivity analysis. Dividing the modified sequestration cost of \$54 per ton CO_2 by the ore demand value (R_{CO_2}/R_X) for the ore in Region 1 results in a cost of \sim \$18 per ton ore. It was

necessary to derive the sequestration cost per ton of ore in order to account for variations in the pretreatment operations, which are mineral-specific and are reported as an energy cost per ton of ore in Table IV. This made it possible to determine an adjusted carbonation cost, including the pretreatment and sequestration costs, for each of the ultramafic mineral-carbonation regions defined in Table II. Multiplying the final adjusted cost per ton of ore by the calculated total ore demand (Table II) provides the total carbonation cost for each region. Dividing the total calculated regional CO_2 emissions (Table II) by the total carbonation costs provides the carbonation cost per ton of CO_2 sequestered. Using this method, the estimated carbonation costs were determined for each ultramafic mineral carbonation region and are reported in Table X. Several key parameters for each region are repeated from Table II for reference. The adjustments made to account for variations in ore grade, grinding intensity, and carbonation conditions were mineral- and/or region-specific and are described below.

The sequestration costs for wollastonite ore in Region 7 were reduced by \$5 per ton ore (to \$13 per ton ore) due to the lower P_{CO_2} (40 atm) utilized in the reactor, based on the P_{CO_2} sensitivity analysis included in the NETL study. However, the pretreatment costs for the wollastonite ore were adjusted for the beneficiation process required due to the lower grade of ore. The size and magnetic separation processes used to produce a wollastonite concentrate were estimated to incur an energy penalty of 4 $\text{kW}\cdot\text{h}/\text{ton}$ ore. Because the beneficiation processes were assumed to be conducted at minus 200-mesh (75 μm) particle size, the grinding costs to that stage increase accordingly, adding 10 $\text{kW}\cdot\text{h}/\text{ton}$ ore to the pretreatment costs. Using the electricity cost of \$0.054 per $\text{kW}\cdot\text{h}$ cited in the NETL study as a basis, the final adjusted carbonation cost is approximately \$14 per ton ore. For simplicity, this adjustment ignores capital costs for the beneficiation operation. Similar adjustments due to lower ore grade and the required beneficiation costs were made for the olivine ores in Region 5, for a final adjusted sequestration cost of \$19 per ton ore.

The non-heat-treated serpentine ores (Regions 2-4, 6) were ground to 80% minus 200-mesh (75 μm), a savings of approximately 70 $\text{kW}\cdot\text{h}/\text{ton}$ of ore compared to the finer grind assumed for the NETL study. Thus, the final adjusted sequestration cost for the non-heat-treated serpentine ores is roughly \$15 per ton ore.

Table X includes two sets of carbonation costs. The first set is for what has been termed standard pretreatment, with the associated costs described above. The second set of carbonation costs refers to the activated pretreatment methodologies, which were defined previously in the discussion for Table II. Ultrafine grinding was utilized for activation of the olivine and wollastonite ores and/or concentrates, while heat-

Table IX. Annual coal consumption, energy generation, CO₂ emissions, ore requirements, and carbonation costs by ultramafic mineral carbonation Region.

| Region | Coal, Mt | Heat value, Btu/lb ¹ | Energy, GW•h (x 1000) | CO ₂ seq., Mt ² | Ore demand, Mt | | Sequestration costs | | | | | | | |
|--------|----------|---------------------------------|-----------------------|---------------------------------------|----------------|------|-------------------------|------|--------------|------|-----------------------------|------|---------|------|
| | | | | | std. | act. | \$/ton ore ³ | | \$, billions | | \$/ton CO ₂ seq. | | \$/kW•h | |
| | | | | | | | std. | act. | std. | act. | std. | act. | std. | act. |
| 1 | 7 | 12300 | 18 | 18 | 53 | 40 | 18 | 26 | 1.0 | 1.1 | 54 | 59 | 0.06 | 0.06 |
| 2 | 4 | 11030 | 9 | 10 | 302 | 64 | 15 | 44 | 4.4 | 2.0 | 427 | 199 | 0.49 | 0.23 |
| 3 | 4 | 11030 | 9 | 10 | 303 | 71 | 15 | 44 | 4.4 | 2.3 | 427 | 222 | 0.49 | 0.25 |
| 4 | 31 | 11360 | 72 | 72 | 2117 | 446 | 15 | 44 | 30.7 | 14.3 | 427 | 199 | 0.43 | 0.20 |
| 5 | 69 | 13080 | 184 | 187 | 552 | 416 | 19 | 27 | 10.3 | 11.1 | 55 | 59 | 0.06 | 0.06 |
| 6 | 85 | 13080 | 220 | 231 | 3971 | 527 | 15 | 48 | 57.7 | 17.9 | 250 | 78 | 0.26 | 0.08 |
| 7 | 28 | 13080 | 75 | 76 | 492 | 259 | 14 | 19 | 6.9 | 4.8 | 91 | 64 | 0.09 | 0.06 |
| Total | 228 | | 587 | 604 | 7790 | 1823 | 15 | 37 | 115.4 | 53.7 | 191 | 89 | 0.20 | 0.09 |

¹ As-fired coal heat value based on primary coal used in each Region, after Babcock & Wilcox (1998).

² Total CO₂ emissions based on coal consumption and carbon content by region (Table II); CO₂ sequestered assumes sequestration of 100% of emissions.

³ Carbonation cost per ton of ore, derived from NETL feasibility by Lyons et al. (2003), with adjustments described in text.

treatment was utilized for activation of the serpentine ores. The grinding energy necessary to grind beyond the 400-mesh (37 µm) size assumed in the NETL study, or the energy required to add a heat-treatment step for the serpentine ores, was reported in Table IV. Using these energies and the \$0.054 per kW•h basis from the NETL study, the adjusted carbonation costs per ton ore and per ton CO₂ were calculated. As described above, the adjustments to the pretreatment costs ignore capital costs for the processing equipment, thus the costs here are lower than would be expected. While it is recognized that these costs could be significant, perhaps as high as the operating costs, proper scaling of equipment would require separate feasibility studies for each Region that are not considered practical at this time. They may not be necessary, because the estimated values included in Table X are intended to provide a relative comparison of carbonation costs between mineral reactants and carbonation Regions, rather than absolute carbonation costs.

DISCUSSION

Carbonation Costs

The carbonation cost summary in Table X illustrates the complex relationship between mineral reactivity, degree of pretreatment, ore demand, and ultimate costs. For example, the ore demand is decreased by roughly 75% for all seven Regions with the addition of the activation step, which more than doubles the cost per ton of ore but reduces the total sequestration cost by over half. The addition of the activation step also reduces the mean sequestration cost for all seven Regions, from \$191 to \$89 per ton CO₂ sequestered, and cut the cost per kW•h in half to \$0.09 per kW•h.

The lowest costs were found for the standard pretreatment olivine ores from Regions 1 and 5, at \$44 and \$55 per ton CO₂ sequestered, respectively. These

costs increased by roughly \$5 per ton CO₂ with the addition of the activation step. Considering the mineral resources described previously for each region, the activation step would only be recommended for the Region-5 olivine ore, due to its limited availability.

The wollastonite ore from Region 7 that was activated by ultrafine grinding has the second lowest carbonation cost, at \$64 per ton CO₂ sequestered. The wollastonite exhibited greater reactivity than any of the other minerals, but its higher R_{CO2} value and lower ore grade, and the ultrafine grinding activation step resulted in slightly higher costs than the olivine ores. However, even with the activation step, the limited wollastonite resource in Region 7 makes it unlikely that the ore could support an *ex situ* mineral-carbonation operation without a significant increase in proven ore reserves.

Of the four regions utilizing serpentine as the mineral reactant, only the antigorite ore from Region 6 has carbonation costs reasonably close to those for the olivine and wollastonite ores. The heat-activated antigorite ore has a carbonation cost of \$78 per ton CO₂ sequestered. This is roughly 35-40% of the cost for the heat-activated lizardite ores from Regions 2-4, and suggests that only the Region 6 serpentine could be reasonably considered for mineral carbonation, with the current process developments, based on economics alone.

CO₂ Balance

The total energy generation by region reported in Table X was included for calculation of the carbonation cost per kW•h, and it was also necessary to determine the net CO₂ avoided by the mineral-carbonation process. The NETL study determined a total energy demand of 352 MW for the baseline process. This baseline value was adjusted to account for the lower energy consumption required for the 1-hour carbonation residence times (all minerals), lower P_{CO2} utilized for wollastonite

carbonation, and the coarser particle size used for the non-heat-treated serpentine ores. The adjusted energy-consumption figures are reported by region in Table X, in GW·h per Mt CO₂ sequestered. The energy consumption required for the mineral-specific pretreatment activation steps is also reported in Table X. The sum of the two is the total mineral carbonation energy consumption for the activated ores.

Assuming the energy required for the mineral-carbonation process was supplied by the same coal-fired power plants generating the CO₂ to be sequestered, the

CO₂ generated by the mineral-carbonation process can be calculated. Subtracting the latter from the total CO₂ sequestered results in the net CO₂ avoided (Table X). The CO₂ avoided with the standard pretreatment methodology for all seven regions, is roughly 76% of the total CO₂ sequestered. Carbonation costs increase accordingly, to roughly \$80 and \$112 per ton of CO₂ avoided for the two olivine ores and the wollastonite ore, respectively. Carbonation costs for the non-heat-activated antigorite and lizardite serpentine ores increase to roughly \$300 and \$500 per ton CO₂ avoided.

Table X. Energy consumption for the mineral carbonation process, with derived CO₂ avoided.

| Region | Energy, GW·h (x1000) | CO ₂ seq., Mt ¹ | Energy consumption, GW·h/Mt CO ₂ seq. | | | CO ₂ avoided, Mt | | Carbonation cost, \$/t CO ₂ avoided | |
|--------|----------------------|---------------------------------------|--|-------------------|-------|-----------------------------|------|--|------|
| | | | std. ² | act. ³ | Total | std. | act. | std. | act. |
| 1 | 18 | 18 | 300 | 333 | 633 | 13 | 7 | 78 | 167 |
| 2 | 9 | 10 | 180 | 2022 | 2202 | 8 | 0 | 537 | NC |
| 3 | 9 | 10 | 180 | 2251 | 2431 | 8 | 0 | 538 | NC |
| 4 | 72 | 72 | 180 | 2022 | 2202 | 59 | 0 | 521 | NC |
| 5 | 184 | 187 | 320 | 333 | 653 | 126 | 63 | 81 | 173 |
| 6 | 220 | 231 | 180 | 829 | 1009 | 187 | 0 | 309 | NC |
| 7 | 75 | 76 | 190 | 239 | 429 | 62 | 43 | 112 | 110 |
| Total | 587 | 604 | | | | 463 | 112 | 249 | 479 |

¹ Total CO₂ emissions based on coal consumption and carbon content by Region (Table II), CO₂ sequestered assumes sequestration of 100% of said emissions.

² Energy consumption for complete sequestration operation, including energy for standard pretreatment methodology and carbonation energy derived from White (2003).

³ Energy for activated pretreatment methodology, mechanical or thermal (from Table IV).

Inclusion of the activation steps dramatically lowers the CO₂ avoided and essentially eliminates the heat-activated serpentine ores from consideration. Inclusion of the heat-activation step results in negative CO₂ avoided, which means more CO₂ is generated than sequestered by the process. The ultrafine grinding step used to activate the olivine and wollastonite more than doubles the olivine carbonation cost, but has little impact on that of the wollastonite. The reason for the latter lies in the lower total energy consumption required for the activated wollastonite compared to the activated olivine. Because the two activated minerals have nearly identical R_x, the lower energy consumption for the activated wollastonite outweighs its higher R_{CO₂} and results in a lower carbonation cost compared to the olivine ores. These results suggest that inclusion of an activation step may be warranted for the wollastonite ore but not recommended for the olivine ores, while heat activation of the serpentine ores is not tenable.

Recoverable Values

During the pilot-scale comminution tests conducted on the olivine and serpentine ores, a wet magnetic-separation step was successfully demonstrated on the minus 200-mesh (75 μm) ground product. A magnetic concentrate representing approximately 5% of the total ground product, with a total iron-oxide grade of roughly 55 wt pct, was produced from each of the serpentine ores.

Using the ore demand figures for Regions 2-4 and 6 and the demonstrated magnetic fraction from the pilot-scale tests, the total iron-ore tonnage was calculated and reported in Table XI. Assuming an iron-ore value of approximately \$30 per ton, the by-product iron concentrate represents an annual revenue value of approximately \$10 billion for the non-heat-activated serpentine ores, and nearly \$2 billion for the activated ores, which would be mined at significantly lower tonnages. This results in modest savings of about \$0.01 per kW·h for the carbonation cost of the serpentine ores, but does little to offset the unfavorable CO₂ balance resulting from the low reactivity of the non-heat activated ores, or the excessive energy consumption required for the heat-activation step.

Table XI. By-product iron ore value.

| Region | Iron ore, Mt | | \$, billions ¹ | | \$/kW·h | |
|--------|--------------|------|---------------------------|------|---------|------|
| | std. | act. | std. | act. | std. | act. |
| 1 | - | - | - | - | - | - |
| 2 | 15 | 3 | 0.5 | 0.1 | 0.44 | 0.22 |
| 3 | 15 | 4 | 0.5 | 0.1 | 0.44 | 0.24 |
| 4 | 105 | 22 | 3.1 | 0.7 | 0.39 | 0.19 |
| 5 | - | - | - | - | - | - |
| 6 | 198 | 26 | 5.9 | 0.8 | 0.24 | 0.08 |
| 7 | - | - | - | - | - | - |
| Total | 335 | 55 | 10.0 | 1.7 | | |

¹ Iron ore value based on \$30 per ton.

CONCLUSION

Carbon dioxide sequestration by an aqueous mineral carbonation process was demonstrated in laboratory-scale batch autoclave tests, using three primary silicate-mineral reactants. These reactants, generally characterized from most reactive to least reactive, include the Ca-silicate wollastonite, Mg-silicate olivine, and hydrated Mg-silicate serpentine. The studies conducted on the Mg-silicate olivine provided the basis for a process feasibility study, which determined a carbonation cost of \$69 per ton of CO₂ sequestered. The study included sensitivity analyses for carbonation reactor residence time and P_{CO₂}, which were utilized to adjust the carbonation costs for more recently developed mineral-specific process improvements. The adjusted carbonation cost for the baseline olivine process is \$54 per ton of CO₂ sequestered.

An energy requirement of 352 MW was determined for a process scaled for the sequestration of 100% of the CO₂ emissions from a 1.3-GW coal-fired electric generation plant (1,100 tons CO₂ per hour). After accounting for the sequestration energy demand, CO₂ avoided was 72% of the total CO₂ sequestered, at a cost of \$78 per ton of CO₂ avoided.

Seven ultramafic mineral carbonation regions, located primarily along both coasts of the conterminous U.S., were identified in the course of the studies. Carbonation costs for the seven regions ranged from \$89 to \$191 per ton of CO₂ sequestered, at an energy cost of \$0.09 to \$0.20 per kW•h, depending on the intensity of mineral-pretreatment operations. The CO₂ avoided for all seven Regions was 76% of the CO₂ sequestered, when using standard pretreatment methodologies.

The studies included an investigation of mineral availability in the seven carbonation regions identified. Total coal-fired electric generation CO₂ emissions within these regions account for roughly 1/3 of the U.S. total, and would require 1.8 to 7.8 Gt per year of silicate ore to carbonate 100% of the emissions, depending on the degree of mineral pretreatment utilized. Two regions utilized olivine, four utilized serpentine, and one utilized wollastonite as the mineral reactant. However, mineral availability followed a reverse trend compared to reactivity, with the order from most abundant to least abundant being serpentine, olivine, and finally wollastonite. Based on ore demand calculations made as part of the study, current resource estimates for wollastonite could not support the regional ore demand, and only one of the regions utilizing olivine could meet the demand for a significant time. Serpentine resources likely exceed the ore demands in three of the four regions but would require dozens of mines on the scale of 50 kt per day to meet the regional demand.

Effective thermal and mechanical mineral activation methodologies were identified that could decrease ore demand by up to 75%. However, energy-consumption determinations for both activation methodologies dramatically impact the process economics and CO₂ balance. Mechanical activation of olivine is not recommended, primarily because it reduces the CO₂ avoided by nearly 50%, and sufficient mineral resources are available in the one region to meet the ore demand without the activation step. However, mechanical activation of wollastonite is recommended, due to its limited availability and the improvement in process economics and minimal impact on CO₂ avoided by inclusion of the activation step. Serpentine carbonation costs were reduced to roughly \$78 per ton of CO₂ sequestered, at an energy cost of \$0.08 per kW•h, with inclusion of a heat-treatment step. However, thermal activation of serpentine, while extremely effective, results in more CO₂ generated than is sequestered by the process, making it an impractical methodology. These calculations assume no heat recovery from the thermal activation step, but plausible heat recovery would be unlikely to dramatically alter the CO₂ balance.

Based on the results of these studies, olivine and wollastonite exhibit the best potential for utilization in an industrial mineral-carbonation process. Current mineral-resource estimates indicate that only olivine could meet the regional ore demands. While serpentine availability makes it the most attractive mineral reactant, having the broadest occurrence and the greatest abundance, current process developments have been unsuccessful at activating the serpentine without a heat-treatment step. The latter can not be supported due to excessive energy demands. Utilization of serpentine may yet find promise as a reactive matrix for geological sequestration, where reaction rate would be defined on the order of years rather than minutes. Preliminary studies of simulated in situ mineral carbonation of serpentine minerals show promise, and may point to viable application of the experience gained from the *ex situ* studies.

REFERENCES

- Babcock & Wilcox (1998). Useful Tables for Engineers and Steam Users, Fifteenth Edition. Babcock & Wilcox Company.
- Barnes, V.E., Shock, D.A., and Cunningham, W.A. (1950). Utilization of Texas Serpentine. The University of Texas, Bureau of Economic Geology, No. 5020.
- Bischoff, J.L. and Rosenbauer, R.J. (1996). The alteration of rhyolite in CO₂ charged water at 200 and 350°C: The unreactivity of CO₂ at higher temperature. *Geochemica et Cosmochimica Acta*, v. 60, no. 20, pp. 3859-3867, Elsevier Science Ltd.
- Bond, F.C. (1952). The Third Theory of Comminution. *Transactions, AIME*, vol. 193, p. 484, American Institute of Mining, Metallurgical, and Petroleum Engineers, Inc., New York.
- Chizmeshya, A.V.G., McKelvy, M.J., Sankey, O.F., Wolf, G.H., Sharma, R., Bearat, H., Diefenbacher, J., and Carpenter, R.W. (2002). Atomic-Level Understanding of CO₂ Mineral Carbonation Mechanisms from Advanced computational Modeling. *Proc., 27th International Technical Conference on Coal Utilization and Fuel Systems*, Coal Technology Association, Clearwater, FL.
- Coleman, R.G. and Irwin, W.P., eds. (1977). North American Ophiolites, IGCP (International Geological Program), State of Oregon, Dept. of Geology and Mineral Industries, Portland, OR, Bulletin 95, 183 pp.
- EIA (2003). Emissions of Greenhouse Gases in the United States 2002, *Energy Information Administration*, Office of Integrated Analysis and Forecasting, US DOE, October 2003, DOE/EIA-0573(2002).
- Goff, F., Guthrie, G., Counce, D., Kluk, E., Bergfeld, D., and Snow, M. (1997). Preliminary Investigations on the Carbon Dioxide Sequestering Potential of Ultramafic Rocks, Los Alamos, NM, Los Alamos National Laboratory, LA-13328-MS.
- Goff, F., Guthrie, G., Lipim, B., Chipera, S., Counce, D., Kluk, E., and Ziock, H. (2000). Evaluation fo the Ultramafic Deposits in the Eastern United States and Puerto Rico as sources of Magnesium for Carbon Dioxide Sequestration, Los Alamos National Laboratory, LA-13694-MS, 36 pp.
- Green, J.C. (1972). North Shore Volcanic Group. In *Geology of Minnesota: A Centennial Volume*, (P.K. Sims and G.B. Morey, eds.), p. 234-332, Minn. Geol. Survey, St. Paul.
- Govier, D. and Arnold, M. (2004). Quantitative Differential Thermal Analysis of Antigorite and Lizardite Serpentine, Internal Report, Albany Research Center Analytical Laboratory.
- Hem, J.D. (1985). Study and Interpretation of the Chemical Characteristics of Natural Water. U.S. Geological Survey Water-Supply Paper 2254, 264 pp.
- Houston, E.C. and Rankin, H.S. (1942). Olivine as a Source of Magnesium Chloride. *Preprint*, Transactions A.I.M.E., Volume 148, American Institute of Mining and Metallurgical Engineers.
- Houston, E.C., and Kerr, H.J. (1945). Magnesium from Olivine by Hydrochloric Acid Extraction Followed by Electrolysis: Pilot-Plant Scale Studies. Report No. 586, Tennessee Valley Authority, Dept. of Chem. Eng., Chem. Research and Eng. Branch, Process Development Division.
- HSC Chemistry for Windows, (1995). Chemical Reaction and Equilibrium Software with Extensive Thermochemical Database. Outokumpo Research Oy, SF – 28101 Pori, Finland.
- Hunter, C.E. (1941). Forsterite Olivine Deposits of North Carolina and Georgia, North Carolina Department of Conservation and Development, Raliegh, NC, Bulletin 41, 117 pp.
- IEA (1999). CO₂ Storage as Carbonate Minerals. Study Prepared by CSMA Minerals Lmtd. Commissioned by International Energy Association, Greenhouse R&D Programme, 124 pp.
- King, E.G., Barany, R., Weller, W.W., and Pankratz, L.B. (1967). Thermodynamic Properties of Forsterite and Serpentine, U.S. Bureau of Mines, RI 6962.
- Lackner, K.S., Butt, D.P., and Wendt, C.H. (1997a). Magnesite Disposal of Carbon Dioxide. Los Alamos National Laboratory, LA-UR-97-660.
- Lackner, K.S., Butt, D.P., and Wendt, C.H. (1997b). Progress on Binding CO₂ in Mineral Substrates. *Energy Conversion Mgmt*, vol. 38, Suppl., pp. S259-S264, Elsevier Science Ltd.
- Lackner, K.S., Butt, D.P., Wendt, C.H., and Ziock, H.J. (1998). Mineral Carbonates as Carbon Dioxide Sinks. Los Alamos National Laboratory, LA-UR-98-4530.
- Lyons, J.L., Berkshire, L.H., and White, C.W. (2003). Mineral Carbonation Feasibility Study, Draft Report, Commissioned by National Energy Technology Laboratroy, 56 pp.
- McKelvy, M.J., Chizmeshya, A.V.G., Bearat, H., Sharma, R., and Carpenter, R.W. (2001). Developing

Mechanistic Understanding of CO₂ Mineral Sequestration Reaction Processes. *Proc., 26th International Technical Conference on Coal Utilization and Fuel Systems*, pp. 777-788, Coal Technology Association, Clearwater, FL.

McKelvy, M.J., Chizmeshya, A.V.G., Bearat, H., Diefenbacher, J., Sharma, R., Carpenter, R.W., and Wolf, G. (2002). Developing a Mechanistic Understanding of Serpentine CO₂ Mineral Carbonation Reaction Processes. *Proc., 27th International Technical Conference on Coal Utilization and Fuel Systems*, Coal Technology Association, Clearwater, FL.

NEXANT (2000). Anaerobic Hydrogen/Electric Power Production and Disposal of CO₂ by Mineral Carbonation. Preliminary Process Viability Assessment, Zero Emission Coal Technology for Zero Emission Coal Alliance, NEXANT, a Bechtel Technology and Consulting Company, 44 pp.

Nguyen, M. T. and Ha, T.K. (1984). A Theoretical Study of the Formation of Carbonic Acid from the Hydration of Carbon Dioxide: A Case of Active Solvent Catalysis. *Journal American Chem. Soc.*, v. 106, pp. 599-602, American Chemical Society.

Nilsen, D.N. and Hundley, G. (1999). Preliminary Feasibility Study of the Sequestration of Carbon dioxide Gas with Minerals: a Study of the LANL Aqueous Process. Albany Research Center, US DOE, DOE/ARC-TR-99-003.

Nilsen, D.N. and Penner, L.R. (2001). Reducing Greenhouse Gas Emissions: Engineering and Cost Assessment of Direct Mineral Carbonation Technology (Process Development Information for the Olivine Process). Albany Research Center, Office of Fossil Energy, US DOE, DOE/ARC-TR-01-015.

O'Connor, W.K., Rush, G.E., Dahlin, D.C., and Reidel, S.P. and Johnson, V.G. (2003). Geological Sequestration of CO₂ in the Columbia River Basalt Group. *Proc., 28th International Technical Conference on Coal Utilization and Fuel Systems*, Coal Technology Association, Clearwater, FL.

Olsen, P.E., Kent, D.V., Cornet, B., White, W.K., and Schlische, R.W. (1996). High-resolution stratigraphy of the Newark rift basin (early Mesozoic, eastern North America). *GSA Bulletin*, v. 108, no. 1, p. 40-77.

Pearre, N.C. and Heyl, A.V. Jr. (1960). Mineral Deposits in the Central Serpentine Districts of the Maryland/Pennsylvania Piedmont Upland, U.S. Geological Survey, Bulletin 1082-K, pp. 707-827.

Platts (2001). U.S. Coal Activity Map, 2001 Edition, *Platts*, a Division of the McGraw-Hill CO., Inc.

Pokrovsky, O.S. and Schott J. (1999). Processes at the magnesium-bearing carbonates/solution interface. II. Kinetics and mechanism of magnesite dissolution. *Geochemica et Cosmochimica Acta*, v. 63, no. 6, pp. 881-897, Elsevier Science Ltd.

Reidel, S.P., Tolan, T.L., Hooper, P.R., Beeson, M.H., Fecht, K.R., Bentley, R.D., and Anderson, J.L., (1989). The Grand Ronde Basalt, Columbia River Basalt Group; Stratigraphic descriptions and correlations in Washington, Oregon, and Idaho. In *Volcanism and Tectonism in the Columbia River Flood-Basalt Province*, (S.P. Reidel and P.R. Hooper, eds.). Geological Society of America, Special Paper 239, p. 21-53.

Reidel, S.P., Johnson, V.G., Spane, F.A. (2002). Natural Gas Storage in Basalt Aquifers of the Columbia Basin, Pacific Northwest USA: A Guide to Site Characterization. PNNL-13962.

Roskill (1990). *The Economics of Olivine 1990*, Second Edition, Roskill Information Services Ltd., London, England.

Sherwood, T.K. and Pigford, R.L. (1952). *Absorption and Extraction*. Second Edition, McGraw-Hill Book Company, Inc.

U.S. Bureau of Mines, Staff (1987). Bureau of Mines Cost Estimating System Handbook (in Two Parts). Part 1. Surface and Underground Mining, IC 9142, 631 pp. Part 2. Mineral Processing, IC 9143, 565 pp.

Virta, R.L. (2001). *Wollastonite*, U.S. Geological Survey Minerals Yearbook –2001.

Wendt, C.H., Butt, D.P., Lackner, K.S., and Ziock, H-J. (1998a). Thermodynamic calculations for acid decomposition of serpentine and olivine in MgCl₂ melts. I Description of concentrated MgCl₂ melts. Los Alamos National Laboratory, Internal Report, LA-UR-98-4528.

Wendt, C.H., Butt, D.P., Lackner, K.S., and Ziock, H-J. (1998b). Thermodynamic calculations for acid decomposition of serpentine and olivine in MgCl₂ melts. II Reaction equilibria in MgCl₂ melts. Los Alamos National Laboratory, Internal Report, LA-UR-98-4529.

Wendt, C.H., Butt, D.P., Lackner, K.S., Vaidya, R., and Ziock, H-J. (1998c). Thermodynamic calculations for acid decomposition of serpentine and olivine in MgCl₂ melts. III Heat consumption in process design. Los Alamos National Laboratory, Internal Report, LA-UR-98-5633.

Zhang, Q., Sugiyama, K., and Saito, F. (1997). Enhancement of Acid Extraction of Magnesium and Silicon from Serpentine by Mechanochemical Treatment. Elsevier Science, *Hydrometallurgy*, v. 45, pp. 323-331.